JGR Atmospheres

RESEARCH ARTICLE
10.1029/2025JD043455

The Short Life of Upvalley Wind in a High-Altitude Valley in the Colorado Rocky Mountains

Bianca Adler[1,2], Vanessa Caicedo[1,3], Brian J. Butterworth[1,2], Laura Bianco[1,2], Christopher J. Cox[2], Gijs de Boer[1,2,4,5], Ethan Gutman[6], Janet M. Intrieri[2], Tilden Meyers[7], Joseph Sedlar[3], David D. Turner[8], and James Wilczak[2]

[1]Cooperative Institute for Research in Environmental Sciences (CIRES), University of Colorado Boulder, Boulder, CO, USA, [2]NOAA Physical Sciences Laboratory, Boulder, CO, USA, [3]NOAA Global Monitoring Laboratory, Boulder, CO, USA, [4]Integrated Remote and In Situ Sensing (IRISS), University of Colorado Boulder, Boulder, CO, USA, [5]Brookhaven National Laboratory, Upton, NY, USA, [6]National Center for Atmospheric Research (NCAR), Boulder, CO, USA, [7]NOAA Air Resources Laboratory, Boulder, CO, USA, [8]NOAA Global Systems Laboratory, Boulder, CO, USA

Abstract Thermally driven upvalley (UV) wind in the upper East River Valley in the Colorado Rocky Mountains often unexpectedly stops in midmorning and reverses back to downvalley (DV) wind. We use a comprehensive observational data set for a nearly two-year long period to analyze the wind system and boundary layer evolution in this high-altitude valley and determine the reason for this early wind reversal. Days with short UV wind predominantly occur during the warm season when the valley floor is free of snow and the convective boundary layer (CBL) grows well above the height of the surrounding ridges. UV wind persists throughout the day only on a few days during the warm season. We link differences in valley wind evolution to wind direction at upper levels at and above ridge height and propose forced channeling mechanisms to describe coupling between valley and upper-level wind when the CBL grows above ridge height. The frequency distribution of upper-level wind direction is such that channeling in the DV direction is favored, which explains the predominance of days with short UV wind. The deep CBL is supported by the presence of a deep weakly stably stratified residual layer with high aerosol content, which is regularly present over the mountain range during the warm season. On days when the CBL does not grow above ridge height, for example, when the valley floor is covered by snow, thermally driven UV wind is able to persist throughout the day independent of upper-level wind direction.

Plain Language Summary The wind in mountain valleys typically follows a distinct diurnal cycle that is driven by heating and cooling of lower atmospheric layers with flow being directed up the valley during the day and down the valley during the night. In the high-altitude East River Valley in Colorado's Rocky Mountain, the upvalley (UV) flow stops early in midmorning on the majority of days when snow cover on the ground is low. This unexpected behavior can be explained by a coupling of the flow in the valley with the flow above the surrounding ridges when a deep well-mixed layer forms in the valley in the morning due to solar heating. Depending on the upper-level wind direction relative to the valley axis, upper-level flow is transported downwards and channeled along the valley in downvalley (DV) or UV direction. The frequency distribution of upper-level wind direction favors channeling in DV direction, which explains why days with short UV wind are more frequent. The valley wind patterns play an important role for the transport of water vapor and pollutants along the valley and above the ridges as well as for the formation of clouds.

Key Points:

- Thermally driven upvalley wind in the East River Valley stops unexpectedly early in midmorning and reverses back to downvalley (DV) wind
- The convective boundary layer height in the valley grows above ridge height allowing coupling of valley and upper-level flow
- Forced channeling of the upper-level flow in DV direction is proposed to explain the early valley wind reversal

Correspondence to:
B. Adler,
bianca.adler@colorado.edu

Citation:
Adler, B., Caicedo, V., Butterworth, B. J., Bianco, L., Cox, C. J., de Boer, G., et al. (2025). The short life of upvalley wind in a high-altitude valley in the Colorado Rocky Mountains. *Journal of Geophysical Research: Atmospheres*, *130*, e2025JD043455. https://doi.org/10.1029/2025JD043455

Received 20 JAN 2025
Accepted 5 MAY 2025

Author Contributions:
Conceptualization: Bianca Adler, Vanessa Caicedo, Christopher J. Cox, Ethan Gutman, Joseph Sedlar
Data curation: Christopher J. Cox, Gijs de Boer, Janet M. Intrieri, Tilden Meyers, Joseph Sedlar, David D. Turner
Formal analysis: Bianca Adler, Vanessa Caicedo
Investigation: Bianca Adler
Methodology: Bianca Adler, Vanessa Caicedo, Brian J. Butterworth, Christopher J. Cox
Project administration: Gijs de Boer
Visualization: Bianca Adler
Writing – original draft: Bianca Adler
Writing – review & editing: Bianca Adler, Vanessa Caicedo, Brian J. Butterworth, Laura Bianco, Christopher J. Cox, Gijs de Boer, Ethan Gutman, Janet M. Intrieri, Joseph Sedlar, David D. Turner, James Wilczak

1. Introduction

Mountainous terrain induces thermally and dynamically driven flows. While thermally driven flows form in response to radiatively driven heating and cooling (e.g., Zardi & Whiteman, 2013), dynamically driven flows form when the large-scale flow interacts with the terrain (e.g., Jackson et al., 2013). The flow in a valley is often channeled along the valley axis, meaning that the wind blows parallel to the valley axis regardless of wind direction at upper levels above ridge height (e.g., Carrera et al., 2009; Eckman, 1998; Weber & Kaufmann, 1998; Whiteman & Doran, 1993). Whiteman and Doran (1993) proposed four physical forcing mechanisms to describe the relationship between upper-level wind direction and valley wind direction. Each physical mechanism can be identified by a unique signal in plots of valley wind direction versus upper-level wind direction. Figure 1 schematizes the different mechanisms for a northwest to southeast oriented valley, which reflects the orientation of the valley under study.

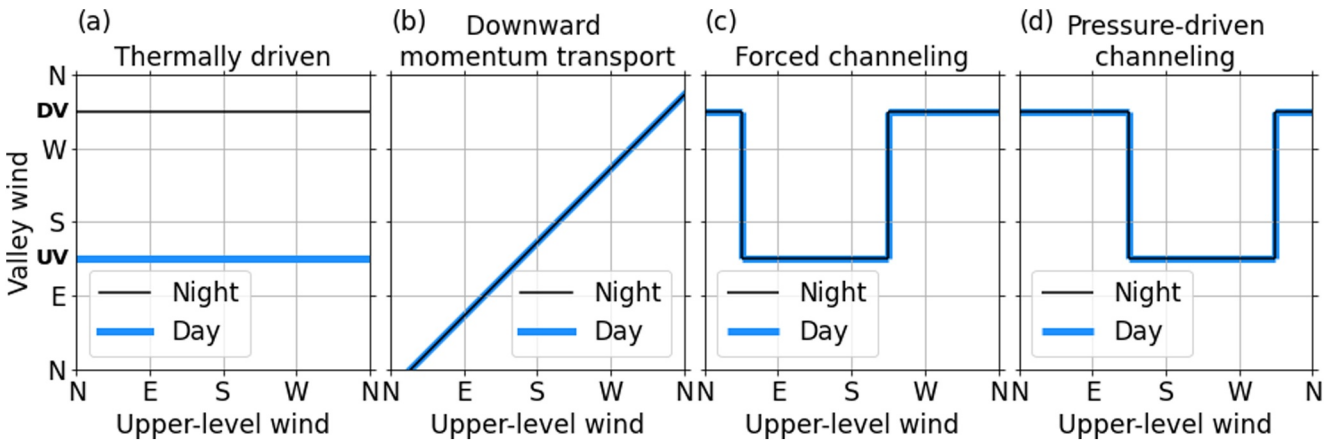

Figure 1. Relationship between upper-level wind and valley wind direction for four possible forcing mechanisms. The valley axis is oriented from northwest to southeast with northwesterly flow being downvalley and southeasterly flow being upvalley, which reflects the conditions present for the East River Valley in this investigation. Adapted from Whiteman and Doran (1993). ©American Meteorological Society. Used with permission.

The first commonly found mechanism is thermally driven. For thermally driven flows, the valley wind direction is independent of upper-level wind direction (Figure 1a). Thermally driven flows are most pronounced under clear-sky fair weather conditions and result from the diurnal cycle of heating and cooling of lower atmospheric layers (e.g., Zardi & Whiteman, 2013). They are characterized by a reversal of wind direction twice per day. Thermally driven valley winds are directed along the valley axis either in the upvalley (UV) direction during day or downvalley (DV) direction during night. They are driven by a hydrostatically produced horizontal pressure difference along the valley axis, which develops when the air in the upper narrower parts of the valley warms or cools faster than the air in the lower wider parts of the valley. This pressure difference reverses sign twice per day and is not to be confused with the pressure-driven channeling mechanism described below. Strength, onset, duration, and depth of the valley winds depend on valley characteristics such as width, depth, length, orientation, and sun exposure. In addition, vegetation, soil moisture, and snow cover impact the surface energy balance and thus thermally driven flows throughout the year. In snow-covered valleys or over glaciers, UV wind during daytime has often been found to be absent. Low-level clouds damp the diurnal cycle of heating and cooling and thus may weaken the signal of thermally driven flows.

For the second mechanism of downward momentum transport, the valley wind direction is similar to the upper-level wind direction with a slight turning of the geostrophic upper-level wind toward lower pressure when approaching the ground (Figure 1b). No channeling along the valley axis occurs. This mechanism is most likely for wide valleys with low sidewalls under unstable or neutrally stratified atmospheric conditions and could be caused by vertical turbulent mixing or gravity waves.

The third mechanism, forced channeling, occurs when the upper-level flow is channeled by the valley sidewalls and aligns with the valley axis within the valley (Figure 1c). The valley wind direction and speed depend on the sign and magnitude of the component of the upper-level wind projected along the valley axis. The valley wind suddenly shifts direction by 180° between UV and DV when the upper-level wind crosses a line normal to the valley axis (i.e., the southwest to northeast direction in Figure 1c). This mechanism is most relevant for relatively narrow valleys with high sidewalls under unstable or neutrally stratified conditions.

For the fourth mechanism, pressure-driven channeling, the valley wind is driven by the component of the geostrophic pressure gradient along the valley axis (Figure 1d). A sudden shift in valley wind direction by 180° occurs when the upper-level wind crosses a line along the valley axis (i.e., the northwest to southeast direction in Figure 1d). This mechanism is likely predominant for wide and shallow valleys under stably stratified conditions.

Although the last three mechanisms do not directly depend on the time of the day like the thermally driven mechanism, differences in stratification between night and day may affect the frequency of their occurrence. For example, forced channeling is more likely to occur during the day when a well-mixed convective boundary layer (CBL) is present in the valley and vertical turbulent mixing allows the downward turbulent transport of upper-

level momentum. As such, the evolution of the atmospheric boundary layer and the CBL depth can have an important impact on the predominance of a certain mechanism during daytime.

The flow in valleys is relevant for a wide range of meteorological research areas. It can impact the distribution of pollutants (e.g., Pal et al., 2014; Steyn et al., 2013), the formation of clouds by transporting moisture above ridges (mountain venting) and by providing a trigger mechanism for convective initiation (e.g., Kirshbaum et al., 2018), the surface energy balance (e.g., Lehner et al., 2021), and the sublimation of snow (e.g., Lundquist et al., 2024).

A nearly two-year long field campaign was conducted in the high-altitude East River Valley in the Rocky Mountains of Colorado with a focus of enhancing weather and water prediction capabilities and understanding the level of fidelity required in simulating land-atmosphere interaction processes to produce unbiased seasonal estimates of the surface energy and water budgets of mountainous watersheds. The field campaign was a collaborative research initiative including efforts associated with the U.S. Department of Energy Atmospheric Radiation (ARM) program Surface Atmosphere Integrated Field Laboratory (SAIL, Feldman et al., 2023) and the NOAA Study of Precipitation, the Lower Atmosphere and Surface for Hydrometeorology (SPLASH, de Boer et al., 2023). In situ and remote sensing instruments were installed at five main sites along the valley axis providing comprehensive atmospheric and hydrologic observations.

The initial analysis of flow patterns in the valley for the different seasons revealed a surprising pattern in valley wind direction in the upper part of the valley on many days especially during warmer summer months. Although a typical thermally driven flow reversal from DV to UV wind was present in the early morning, the UV wind often ended before noon and the flow shifted back to the DV direction; this “early reversal” is unexpected for typical thermally driven flow conditions. The aim of this study is (a) to characterize the boundary layer evolution and vertical structure on days with and without the early reversal of UV wind and (b) to identify physical processes responsible for the different observed behaviors.

The manuscript is structured as follows: Section 2 describes the investigation area and the data used in this study. In Section 3, the seasonal and diurnal cycles of near-surface boundary layer conditions are presented and criteria for the selection of study days are described. Section 4 contrasts boundary layer evolution and structure on days with and without the early reversal of UV wind, and Section 5 investigates the relationship between the valley and upper-level wind directions. The manuscript concludes with a discussion on the role of boundary layer depth and with a comparison of our findings to research in other mountain valleys (Section 6) and a summary (Section 7).

2. Investigation Area and Data

2.1. Investigation Area

The East River Valley is embedded in the East River Watershed, which is a mountainous headwater catchment of the Colorado River Basin and is located near Crested Butte in Colorado's Rocky Mountains (Figure 2a). The land cover in this area includes a mix of evergreen and deciduous forest, grasslands, and barren land as visible in the photograph in Figure 2d. In this study, we use meteorological data from four measurement sites in the valley (Figure 2b) with a focus on the three sites in the upper part of the valley (Avery Picnic, Gothic, and Kettle Ponds). The fourth site, Roaring Judy, was located about 35 km further down the valley. At Gothic, the second ARM Mobile Facility (AMF2) was deployed for the SAIL campaign (Feldman et al., 2023) providing detailed, vertically resolved observations of temperature, wind, turbulence, and aerosol content in the boundary layer. The other three sites were operated for the SPLASH campaign (de Boer et al., 2023) and mainly provided near-surface meteorological observations. The valley narrows from a few kilometers to less than 1 km at Avery Picnic, the site furthest north.

To estimate a characteristic ridge height in the area, we selected an approximately 30 km × 30 km horizontal box covering the high terrain around the upper part of the valley. The terrain data have a horizontal resolution of 30 m. We then determined the 90% quantile and selected grid points exceeding this threshold. These grid points, which we considered as representative of the high terrain, had a mean of 3.9 km and a maximum of 4.3 km above mean sea level (MSL). With a valley floor altitude of more than 2.8 km above MSL in the upper part of the valley, we characterized the ridge height as 1–1.5 km above this valley floor.

The valley axis in the upper part is generally aligned northwest to southeast but important smaller scale terrain features are present as well (Figure 2c). A few kilometers UV (north) of Avery Picnic the valley forks with a

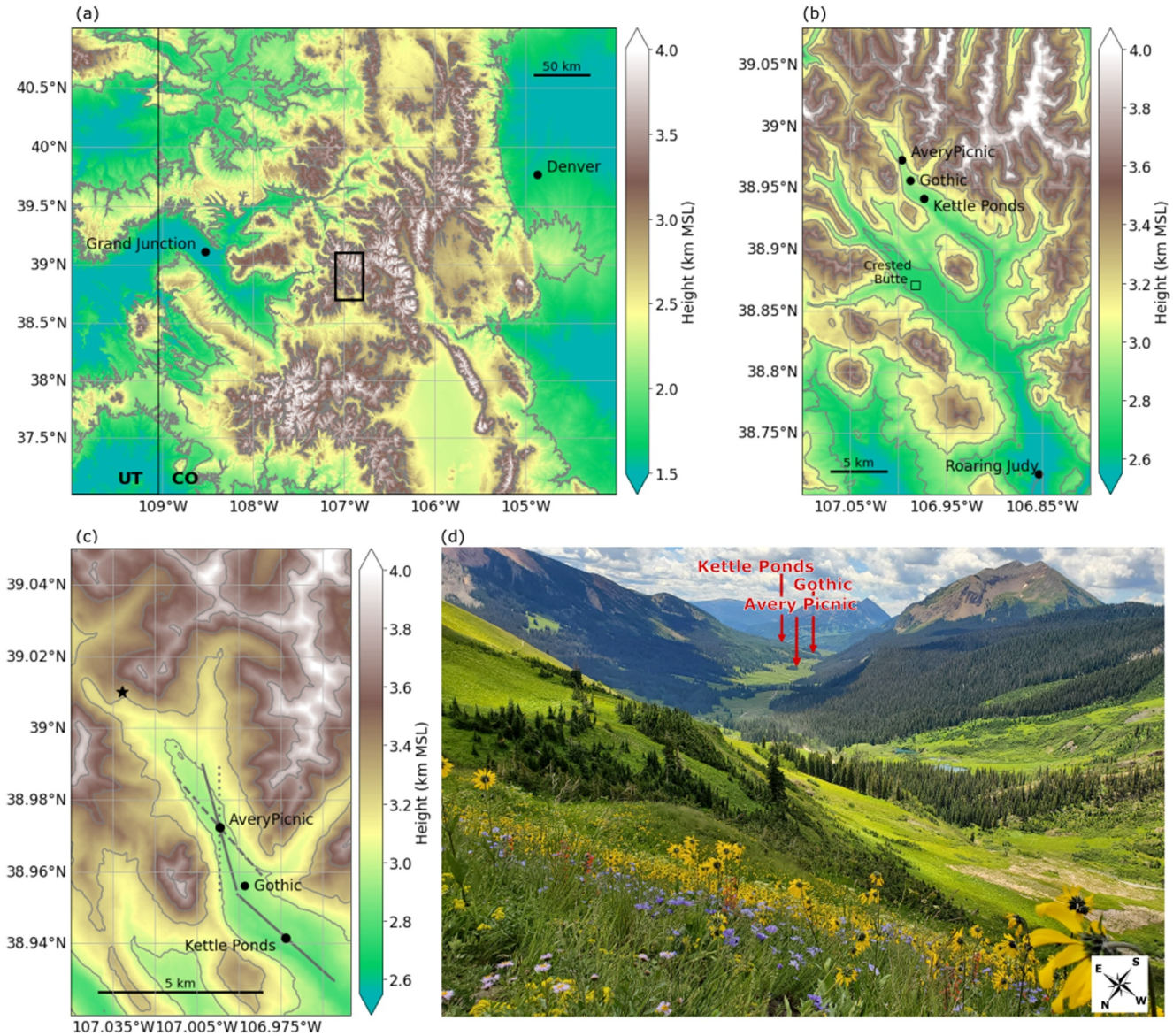

Figure 2. Terrain height based on 30-m resolution elevation data from the Shuttle Radar Topography Mission of (a) the Rocky Mountains in the western part of Colorado, (b) the investigation area in the East River Valley, and (c) zoomed in on the upper part of the East River Valley. The black rectangle in (a) indicates the location of the investigation area. In (c), the solid gray line at Kettle Ponds marks the mean valley axis determined from near-surface up and downvalley (DV) wind measurements. At Avery Picnic, the three different valley axes are indicated: the dotted line is based on nocturnal DV wind measurements, the solid line is based on daytime upvalley wind measurements, and the dashed line marks a subjective valley axis based on the terrain. (d) Photograph taken by the first author in July 2022 on the slope in the upper part of the western fork (location indicated by the star in (c)) looking DV.

northerly fork and a northwesterly fork being in line with the main valley axis. Gothic is located at the mouth of a tributary valley extending to the northeast. This tributary valley was found to affect the near-surface atmospheric conditions at this site making them unrepresentative for the main valley conditions. Since the impact of the tributary valley diminishes with height, we still are confident using boundary layer profiles at this site for our analysis.

Based on near-surface wind direction measurements at Avery Picnic and Kettle Ponds, we estimated the direction of the valley axis at these sites (indicated by the gray lines in Figure 2c). At Kettle Ponds, this along-valley direction was very similar for up and DV flow and agreed fairly well with the alignment of the sidewalls. At Avery Picnic, we found a difference of more than 20° between daytime UV and nocturnal DV flow direction with DV flow being northerly and UV flow being more south-southeasterly. The northerly DV flow near the surface is

likely related to cold-air drainage from the northerly fork. The valley axis for UV flow is indicated by the solid gray line and the one for DV flow by the dotted gray line in Figure 2c. When looking at the sidewall orientation a few kilometers up and down from Avery Picnic, one might expect an even more southeasterly to northwesterly orientation of the valley axis and we additionally indicate this subjective terrain-based valley axis by the dashed gray line in Figure 2c.

2.2. Data

2.2.1. Surface Observations

We used near-surface observations of temperature, humidity, horizontal wind, air pressure, shortwave incoming and outgoing radiation, and turbulent kinetic energy (TKE) from two sites in the upper part of the valley, Avery Picnic and Kettle Ponds. Measurement heights were 3 m above ground level (AGL) at Avery Picnic and Kettle Ponds for temperature, 3 m AGL at Avery Picnic and 5 m AGL at Kettle Ponds for humidity, and 4.6 m AGL at Avery Picnic and 10 m AGL at Kettle Ponds for wind and turbulence. Turbulent kinetic energy was computed over 30-min time periods, all other variables were averaged over 10-min periods. All data at Avery Picnic were obtained from an Atmospheric Surface Flux Station (ASFS, Cox et al., 2025). Radiation measurements at Kettle Ponds were collected by a mobile SURFRAD-like station (Sedlar et al., 2022), and all other data came from a 10-m flux tower. All surface heights vary in the winter with the development of a 1–2 m snowpack. To estimate albedo, we computed daily averages of broadband shortwave downward and shortwave upward radiation fluxes when the solar zenith angle was less than 85° before taking the ratio. From Roaring Judy, we used near-surface pressure and temperature observations at 2 m AGL to compute the along-valley pressure gradient. Details on the platforms and sensors can be found in the references given above and in the metadata for the individual data sets (see Data Availability Statement).

2.2.2. Thermodynamic Profiler

At Gothic, an infrared spectrometer, the Atmospheric Emitted Radiance Interferometer (AERI, Knuteson et al., 2004a, 2004b), was operated. Thermodynamic profiles were retrieved every 5 min from the observed instantaneous radiances using the optimal estimation physical retrieval TROPoe (Turner & Blumberg, 2019; Turner & Löhnert, 2014, 2021). The TROPoe version used includes the latest improvements described by Adler et al. (2024). Blumberg et al. (2015) and Bianco et al. (2024) evaluated such retrieved profiles against radio soundings and found a good agreement in the boundary layer. Besides infrared radiances, additional input data in TROPoe included cloud-base height from a colocated ceilometer, temperature, and water vapor mixing ratio from in situ near-surface observations, brightness temperature at two frequencies (23.8 GHz, 31.4 GHz) from a microwave radiometer, and temperature and water vapor mixing ratio profiles from twice-daily radiosondes at Gothic. In addition to this temporally resolved input data, the retrieval requires climatological priors of temperature and humidity which we computed from operational radiosondes launched near Denver, Colorado. The retrieval produces an estimate of temperature and water vapor profiles with 55 vertical levels each from the surface up to 17 km with the distance between levels starting at 10 m and increasing with height as well as liquid water path (LWP). To reduce some of the temporal noise, we averaged the retrieved profiles over 10 min intervals before using them in our analysis.

From the 10-min averaged virtual potential temperature profiles, we computed CBL depth using the parcel method (e.g., Seibert et al., 2000). Although the CBL depth derived from TROPoe profiles generally agree well with those derived from radiosonde profiles (Duncan et al., 2022), the retrieval may not be able to capture the strength and location of an elevated temperature inversion like at the top of a multi-kilometer deep residual layer. This is because the information content of the AERI decreases with height resulting in an increase in vertical resolution, that is, in the vertical layer depth for which a retrieved temperature value is representative. This limitation hindered us to directly determine the height of the inversion topping the nocturnal residual layer from TROPoe retrievals and instead we used the top of the aerosol layer detected by high spectral resolution lidar (HSRL) (Section 2.2.3) as a proxy.

2.2.3. High Spectral Resolution Lidar

A HSRL was deployed at Gothic (Goldsmith, 2016). It emits a laser beam at a wavelength of 532 nm and provides separated measurements of molecular and particulate scattering (Eloranta, 2005). In this study, we used profiles of

absolutely calibrated particulate backscatter cross section to visualize the aerosol layer and to detect its depth. The backscatter cross section profiles were available with a temporal resolution of 30 s and a vertical resolution of 30 m with the first range gate at 60 m AGL. They were averaged over 10-min intervals for visualization and for aerosol layer depth detection. Gradients in backscatter profiles corresponding to aerosol layers were identified using a Haar Wavelet transform approach following a method similar to Caicedo et al. (2020). This technique detects significant changes in backscatter above 900 m for nighttime and 990 m for daytime to avoid uncertainty in the near-surface overlap region and to prevent the retrieval from picking up weak gradients close to the surface. An upper limit of 5,000 m was used to minimize noise at higher altitudes and prevent erroneous estimates. The approach also ensured continuous retrieval of the well-mixed daytime aerosol layer by applying temporal and continuity criteria.

2.2.4. Doppler Lidar

A Doppler lidar was operated at Gothic (Newsom & Krishnamurthy, 2022). It detected the line of sight radial velocity of scatterers using the Doppler frequency shift with a temporal resolution of 1 s and a spatial resolution of 30 m. The scan strategy consisted of a combination of range-height-indicator scans (every 60 min), plan-position scans (every 15 min), and vertical stare for the remaining time. From the vertical stare profiles, vertical velocity variance profiles were routinely computed for 10-min intervals and from the plan-position scans, horizontal wind profiles were retrieved. Unfortunately, due to a lack of scatterers in the valley and poor data quality, the vertical range of the horizontal wind profiles was often limited. They did not extend regularly to ridge height, making them unsuitable for the characterization of the upper-level flow at and above ridge height in our composite analysis.

2.2.5. Ceilometer

We used information on cloud-base height from a ceilometer deployed as part of the mobile SURFRAD observing suite (Sedlar et al., 2022) at Kettle Ponds to compute 10-min temporal cloud-base height fraction for cloud bases below 3 km AGL. Standard manufacturer processing of the attenuated backscatter profiles was employed to identify cloud base height locations in the vertical column above the ceilometer.

2.2.6. Radiosondes

Radiosondes were launched at Gothic twice daily at 00:00 and 12:00 UTC, which corresponds to 05:00 and 17:00 Mountain Standard Time (MST), providing thermodynamic and wind profiles throughout the troposphere (Holdridge, 2020). We also compared the radiosonde profiles at Gothic to radiosonde profiles launched operationally at the same times at Grand Junction, approximately 140 km west of Gothic (location in Figure 2a), to investigate the spatial variability in boundary layer conditions on a larger scale. Unfortunately, no operational radiosondes were launched at the long-term radiosonde station in Denver on the plains east of the mountains after July 2022 due to the worldwide helium shortage.

2.2.7. Terra Satellite

To get information on the temporal evolution of spatial snow coverage in the area of the East River Valley (38.5–39.05°N, 107.7–106.7°W), we used the normalized difference snow index (NDSI) from MODIS on-board of the Terra satellite (Hall & Riggs, 2021). Snow-covered surfaces typically have a high reflectance in visible bands and low reflectance in shortwave infrared bands. The NDSI reveals the magnitude of this difference. A pixel with $0 < \text{NDSI} \leq 1$ was considered to have some snow present and a pixel with $\text{NDSI} = 0$ was considered to be snow free land surface. NDSI was available daily on a regular grid with 500 m spacing. We computed a mean daily NDSI for the investigation area when valid NDSI data were available for at least 50% of the pixels and not obscured by clouds.

2.2.8. RAP Model Analysis

Because the Doppler lidar did not reliably provide horizonal wind measurements at ridge-height, we used data from the analysis of the operational Rapid Refresh (RAP, Benjamin et al., 2016) weather prediction model to characterize the upper-level wind. The RAP is an hourly updated forecast system that assimilates a variety of airborne, ground-based and satellite observations. With a horizontal grid spacing of 13 km, the mountainous

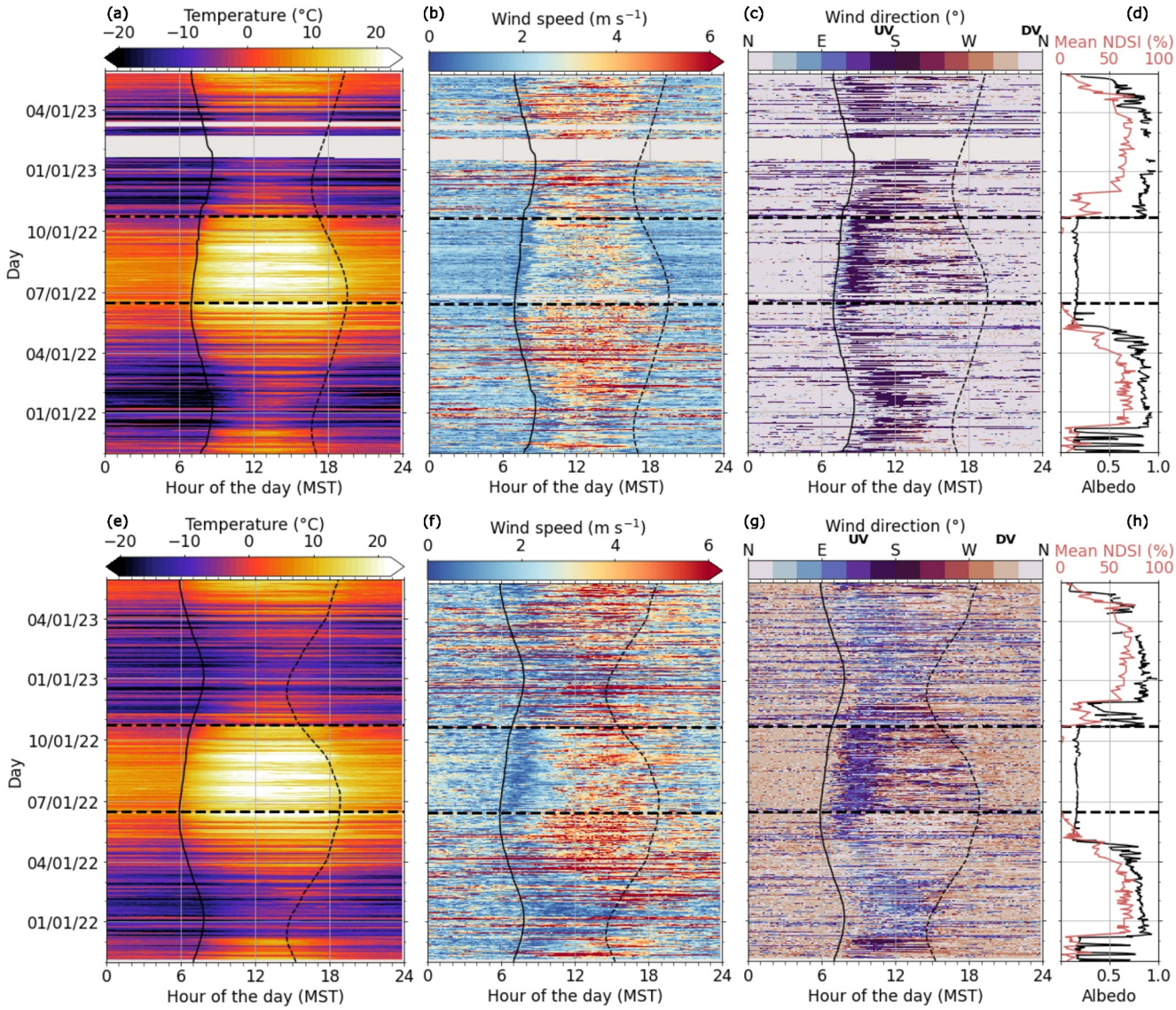

Figure 3. Daily evolution of near-surface (a, e) temperature, (b, f) wind speed, and (c, g) wind direction from November 2021 to June 2023. (d, h) Time series of daily local albedo and area-averaged normalized difference snow index (NDSI). Gaps in NDSI are linearly interpolated. The top row shows Avery Picnic and the bottom row Kettle Ponds. The thin solid and dashed lines mark local sunrise and sunset, respectively. The horizontal thick dashed lines enclose the warm season used for further analysis. Periods with missing data appear in light gray.

terrain in the RAP is smoothed and we do not expect the RAP to resolve the terrain induced flows in the East River Valley. Thus, we only analyzed model data above the maximum ridge height at 4.3 km MSL. We selected a grid point close to the upper East River Valley where the model terrain height was similar to the actual valley floor height and used the twice daily radiosonde profiles to evaluate the RAP horizontal wind at 4.3 km MSL. High correlation coefficients of 0.82 for wind direction and 0.84 for wind speed enhance our confidence in using model data for the upper-level flow characterization and suggest that the main conclusions of the study are not compromised by the lack of suitable upper-level flow observations.

3. Boundary Layer Characteristics in the Valley

3.1. Seasonal and Diurnal Cycle of Temperature, Wind, and Snow Cover

Figure 3 shows the seasonal and diurnal cycle of near-surface temperature, wind speed, and wind direction at Avery Picnic and Kettle Ponds from November 2021 to June 2023. As an indication of snow cover, time series of

local albedo and area averaged NDSI are also displayed (Figures 3d and 3h). By looking at both variables, differences in snow cover locally at the sites and in the overall valley become visible. In 2021, snow cover in the valley sharply increased at the beginning of December after a multiday snowfall event (Adler et al., 2023) and remained continuously high until the beginning of the melting period in spring 2022. The melt-out at Kettle Ponds, visible in the transition to low albedo values, happened around 3 May 2022 and about 10 days later at Avery Picnic. The area-averaged NDSI at this time was above 15% indicating that areas higher up in the valley were still snow covered. NDSI decreased until around June 15 and remained low (<1%) until October, only interrupted by a minor snowfall event at the end of September that temporarily increased NDSI. The first major snowfall event occurred again on 23 October 2022 marking the beginning of the second snow season. While snow partially melted in the valley and Kettle Ponds after this event, it persisted at Avery Picnic, as indicated by consistently high albedo values there (Figure 3d). We will refer to the period between 15 June and 23 October 2022 when the NDSI is low (<1%) as the warm season in the following.

The seasonal and diurnal cycle in temperature (Figures 3a and 3e) is strongly correlated with snow cover (Figures 3d and 3h) with much lower temperatures and a damped diurnal cycle when snow cover in the valley was high. As soon as the snow had melted at a site, daytime temperatures regularly exceeded 15°C and a strong diurnal cycle was present. Wind direction also showed a strong diurnal cycle that depended on season (Figures 3c and 3g). DV flow dominated during the night (northerly flow at Avery Picnic and northwesterly flow at Kettle Ponds). About 1 hr after sunrise (thin solid lines in Figure 3), the flow turned to UV and slowly increased in strength (Figures 3b and 3f). This turn to UV was most pronounced during the warm season, which is consistent with the findings by Adler et al. (2023) and the often observed absence of UV wind in snow-covered valleys (Zardi & Whiteman, 2013). On many days, especially during the warm season, the flow turned back to DV in mid to late morning after only a few hours of UV wind and remained DV until sunset and throughout the night. This early shift back to DV direction is unexpected. The wind system in the upper part of the East River Valley shows a clear indication to be thermally driven at night and in the early morning, that is, nocturnal DV wind and a shift to UV wind after sunrise. If thermally driven flows were dominant throughout the day, an UV flow would be expected to persist until the evening when along-valley temperature and pressure gradients reverse. The early shift back to DV wind cannot be explained by a typical thermally driven flow system. On the other hand, the very regular timing of the wind shift back to DV in mid to late morning suggests that the diurnal cycle of the boundary layer evolution and CBL growth play an important role. In the following section, we will focus on the warm season, when the signal was strongest, and investigate what causes this early reversal to DV wind in the morning in the upper part of the valley.

3.2. Selection of Thermally Driven Days During the Warm Season

We aim to investigate the early reversal of UV wind on days during the warm season, which show a clear signal for thermally driven flow in the morning. We hence selected days that showed a distinct shift from DV wind before sunrise to UV wind after sunrise. For a day to be classified as thermally driven, we required persistent DV wind at least 2 hr before sunrise and a shift to UV wind within 3 hr after sunrise at both the Avery Picnic and Kettle Ponds sites; these criteria were selected subjectively based on the collective observed diurnal wind conditions. In case of data gaps at one of the sites, the criteria only had to be fulfilled at the other site. In total, we identified 102 days (more than 75% of all days during the warm season) that fulfilled these criteria. These cases were distributed approximately randomly with no discernible pattern throughout the warm season (Figure 4). The only large gap in selected days occurred in late September and early October when an early snowfall event temporarily increased NDSI (Figures 3d and 3h).

Because our only criteria for the day selection was the wind reversal in the morning, we did not explicitly exclude days with clouds. Although many of the selected days were mostly clear sky during the first half of the day, clouds were present on some days (Figure 4b). By impacting the surface energy balance, clouds in the morning could mask or delay thermally driven wind shifts. However, LWP was usually low with LWP < 40 g m^{-2} (Figure 4c), which may explain why we still observed a thermally driven wind reversal from DV to UV wind in the morning on those days due to radiative heating and cooling. In late morning, cloud cover and LWP often increased (Figures 4b and 4c), which is likely related to moist convection triggered by converging flows over the slopes and ridges. Moist convection and especially precipitating cells may strongly impact the wind field in the valley by impacting spatial heating and cooling patterns and by producing cell-induced circulations as well as cold air outflows. Since the reversal of UV wind usually occurred before or at the same time when cloud cover increased,

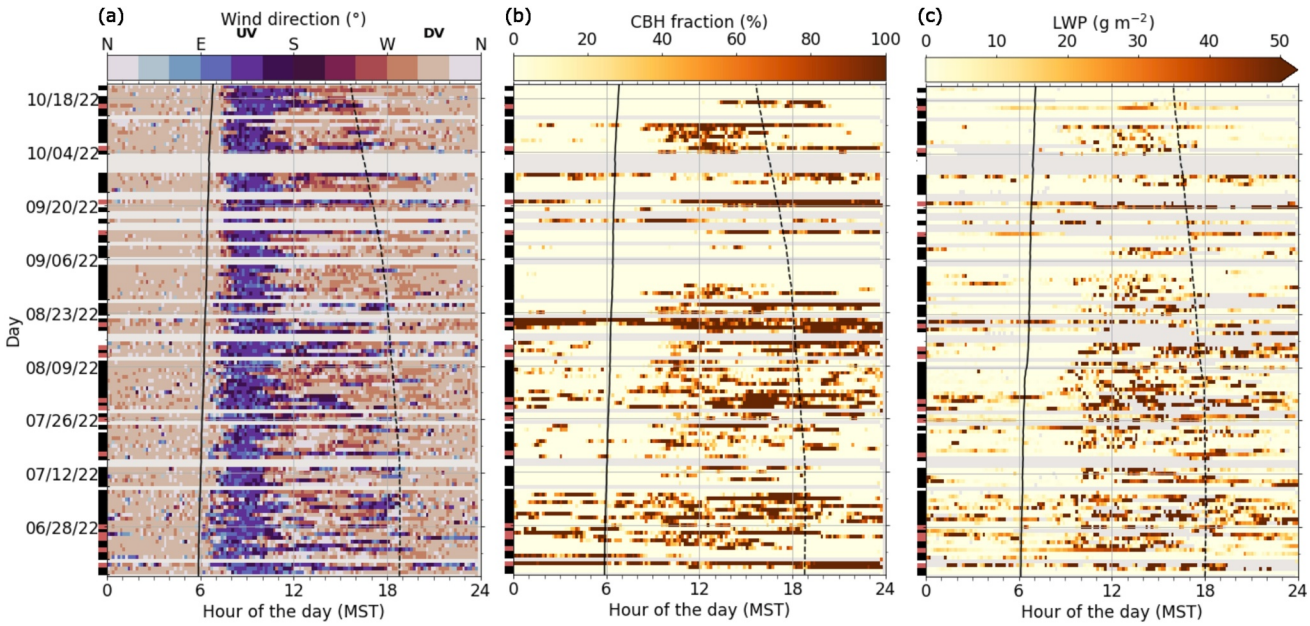

Figure 4. Daily evolution of (a) near-surface wind direction at Kettle Ponds, (b) 10-min cloud-base height fraction for cloud bases below 3 km above ground level at Kettle Ponds, and (c) liquid water path (LWP) at Gothic on thermally driven days during the warm season. The thin solid and dashed lines show sunrise and sunset, respectively. Black and red bars at the left of the *y*-axis indicate short and long upvalley (UV) wind days, respectively (for selection criteria see text). Periods with nonthermally driven winds or missing data appear in light gray. Approximate downvalley and UV wind direction are indicated in (a).

we deem clouds as less relevant for the process causing the flow reversal and leave the investigation of clouds and moist convection and how they relate to the wind reversal for future studies.

The temporal evolution of wind direction shows distinct differences during the selected thermally driven days (Figure 4a). On many of the days, flow reversed from UV to DV in mid to late morning as already noted in the previous section. However, on a few days, UV wind persisted throughout the day until around sunset. We further separated the thermally driven days into cases with short UV wind lasting for less than five consecutive hours (hereafter short UV wind) and cases with long UV wind lasting for more than 5 hr (long UV wind). We found that the threshold of 5 hr was well suited to distinguish between the types of days, since UV wind cases persisting for more than 5 hr typically persisted throughout the length of the day. This separation resulted in 79 days with short UV wind and only 16 days with long UV wind. Since we required that both the Avery Picnic and Kettle Ponds sites, if available, fulfilled the temporal criteria, the sum of short and long UV wind days is less than the total number of thermally driven days. Days with short and long UV wind are indicated by the black and red bars at the left *y*-axis in Figure 4. It is important to note that short and long UV wind days occurred throughout the warm season, indicating that factors such as solar radiation, vegetation, or land cover are not decisive for their occurrence.

The composites of the frequency distribution of wind direction in Figure 5 clearly show distinct flow characteristics on short and long UV wind days. The nocturnal DV wind and the morning shift to UV wind was similar on both types of days and occurred between 07:00 and 08:00 MST. The transition was slightly blurred due to sunrise spanning a 60-min time period between 06:00 and 07:00 MST during the warm season (thin solid line in Figure 4). The flow shifted back to DV in mid to late morning (between around 10:00 and 11:00 MST) on short UV wind days only and remained very consistent for the rest of the day especially at Avery Picnic (Figures 5a and 5c). At Avery Picnic, DV flow during the night was almost exactly northerly, whereas DV flow during the day had a slight westerly component. This indicates that the cold air drainage from the northerly fork (Figure 1c) driving the DV flow during the night was not responsible for the DV flow during the day. The spread in wind direction was generally a bit larger in Kettle Ponds, which might be related to the wider less confined valley at this site (Figure 2c). On long UV wind days, the UV wind generally persisted until late afternoon before it turned back to DV (Figures 5b and 5d). The relatively large variability in wind direction, especially during the second

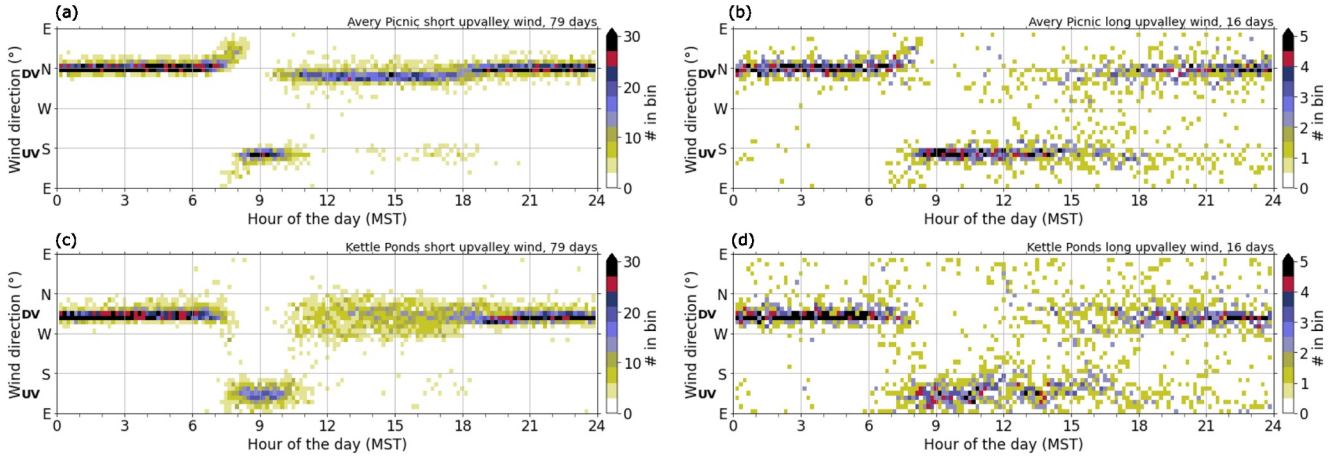

Figure 5. 24-hr composites of the frequency distribution of wind direction at Avery Picnic (a, b) and Kettle Ponds (c, d) for the (a, c) 79 short and (b, d) 16 long upvalley (UV) wind days during the warm season (for selection criteria see text). Approximate downvalley and UV wind directions at each site are indicated. The bin sizes are 10° and 10 min, respectively. Note the different range of the colorbars.

half of the day, might be related to moist convection and precipitation affecting the valley flow and to the smaller sample size on these days.

4. Boundary Layer Conditions on Short and Long Upvalley Wind Days

4.1. Examples of Short and Long Upvalley Wind Days

In this section, we will analyze the boundary layer conditions for a typical short and long UV wind day using 7 August and 12 August as examples. On 7 August, UV flow ended at 09:00 MST (Figure 6a), while it persisted until late afternoon on 12 August (Figure 6b). Horizontal wind speed was variable with time and no distinct differences are visible between these days (Figures 6e and 6f). Strong surface inversions were present on both days during the night and were slowly eroded by a growing CBL after sunrise at around 06:00 MST (Figures 7a and 7b). A less stably stratified residual layer was present above the nocturnal surface inversion whose top coincided with the top of the layer with high aerosol loading (Figures 7c and 7d). Near-surface temperature and water vapor mixing ratio increased at both sites and both days with the onset of radiative heating after sunrise (Figures 6c, 6d, 6g, and 6h). About 1–2 hr after sunrise, while the CBL was still eroding the nocturnal surface inversion (Figures 7a and 7b), near-surface wind direction at Avery Picnic and Kettle Ponds very nicely shows the shift from DV to UV wind (indicated by vertical solid lines in Figures 6 and 7). When the CBL top reached the less stably stratified residual layer, CBL growth accelerated and the CBL depth increased by more than 1 km within a 30 min period to around 1.5 km (Figures 7a and 7b). This happened at approximately 08:30 MST on August 7 and 10:00 MST on August 12. After that, the CBL continued to grow at a slower rate up to the top of the deep aerosol layer (Figures 7c and 7d).

During the rapid growth period of the CBL, distinct changes in near-surface and boundary layer conditions occurred on both days. First clouds formed at the top of the CBL above the valley center (high backscatter values in Figures 7c and 7d), near-surface water vapor mixing ratio decreased sharply by around 2 g kg^{-1} (Figures 6g and 6h) and TKE abruptly increased (Figures 6i and 6j). Turbulence not only increased near the surface but throughout the whole CBL, as is visible in the vertical velocity variance profiles in Figures 7e and 7f. This was also the time when the UV wind turned back to DV on the short UV wind day (Figure 6a).

We computed the horizontal pressure difference between Roaring Judy in the lower part of the valley and Avery Picnic and Kettle Ponds in the upper part of the valley after reducing the pressure at Roaring Judy to the altitude of the higher sites and removing a remaining offset (Figures 6k and 6l). Typically, the horizontal pressure difference shows a strong diurnal cycle with a maximum in the early morning and minimum in the late afternoon on days with thermally driven valley wind (e.g., Giovannini et al., 2017; Lehner et al., 2019). In the East River Valley, the pressure difference showed the expected decrease in the early morning when the valley atmosphere warmed faster in the upper parts of the valley. This can explain the observed onset of an UV wind. The horizontal pressure

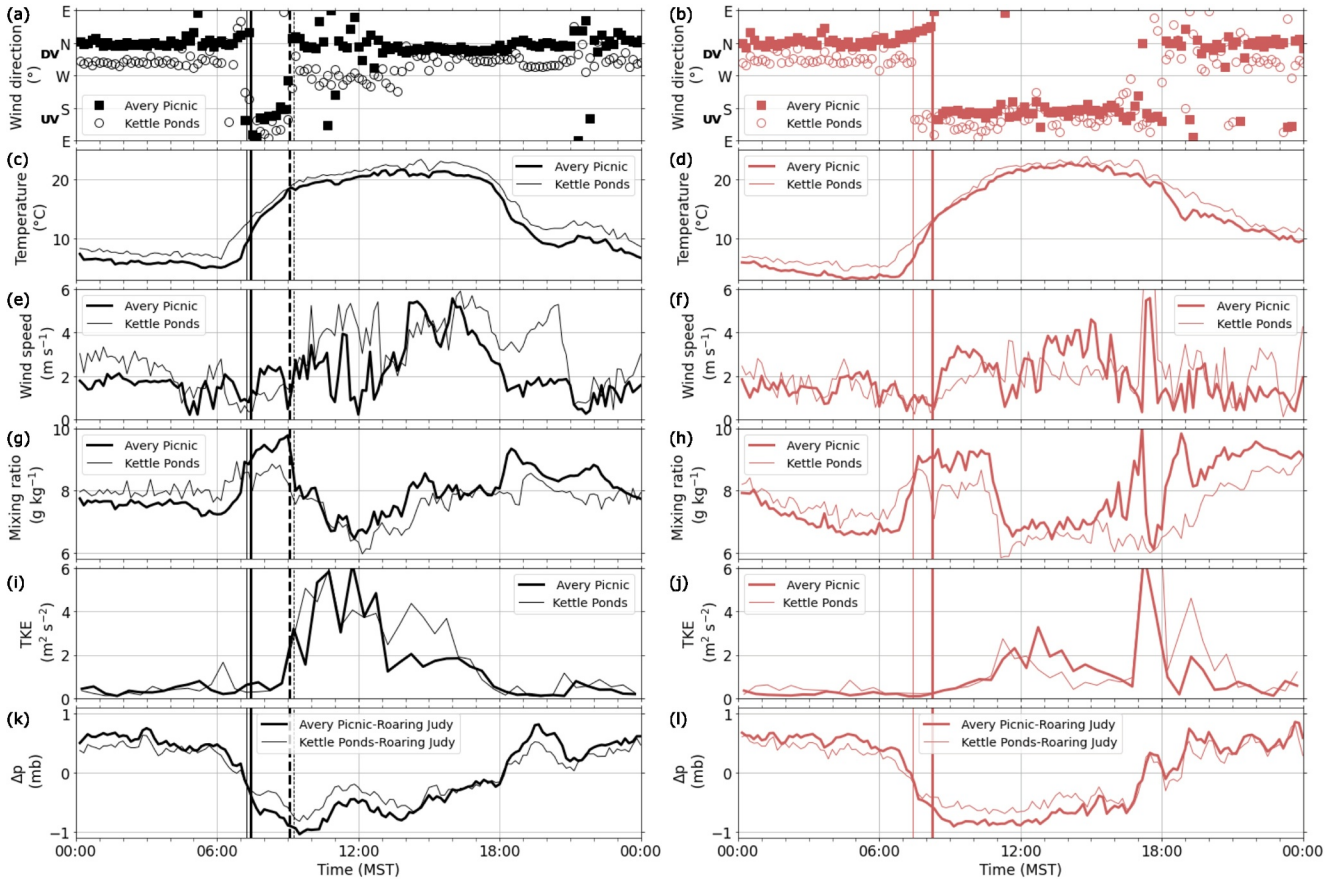

Figure 6. Time series of near-surface (a, b) wind direction, (c, d) temperature, (e, f) horizontal wind speed, (g, h) water vapor mixing ratio, (i, j) turbulent kinetic energy, and (k, l) along-valley pressure difference on a short upvalley (UV) wind day in black (7 August 2022, left column) and a long UV wind day in red (12 August 2022, right column). The vertical solid thick and thin lines indicate the objectively determined onset of UV wind at Avery Picnic and Kettle Ponds and the vertical dashed thick and thin lines the shift back to downvalley (DV) wind on the short UV wind day. Approximate DV and UV wind directions are indicated in (a, b).

difference started to deviate from the typical temporal evolution in mid to late morning when the CBL grew above ridge height on both days. The pressure difference then reached a minimum and stayed roughly constant or slightly increased throughout the afternoon but remained negative. Assuming that the large-scale pressure changes above ridge height were the same in the lower and upper part of the valley, this means that now the valley atmosphere in the lower part warmed at the same rate or even faster than in the upper part, maintaining or reducing the existing temperature and hence pressure difference.

Boundary layer conditions in the valley are very similar on both days and give no indication on which processes might cause the early reversal of UV wind on 7 August. We hence inspected the horizontal flow at and above ridge height using the RAP model analysis. Clear differences are evident in wind direction during the morning and early afternoon with westerly flow on 7 August and southeasterly flow on 12 August (Figures 7g and 7h). According to the concept of Whiteman and Doran (1993), upper-level westerly flow can result in forced channeling in DV direction and upper-level southeasterly flow in forced channeling in UV direction for a northwest to southeast oriented valley (Figure 1c). Based on the observational evidence, we hypothesize that strong downward mixing of momentum occurred when the CBL grew above ridge height into the upper-level flow resulting in forced channeling on both presented days. On 7 August, the upper-level flow direction was such that the flow was channeled in the DV direction resulting in the early end of the UV wind. On 12 August, the observed UV wind during the day could be thermally driven. However, the evolution of the along-valley pressure gradient deviated from the typical thermally driven pattern found in other valleys (no decrease after midmorning). This suggests that forced channeling of upper-level momentum was present as well and superimposed on the UV wind.

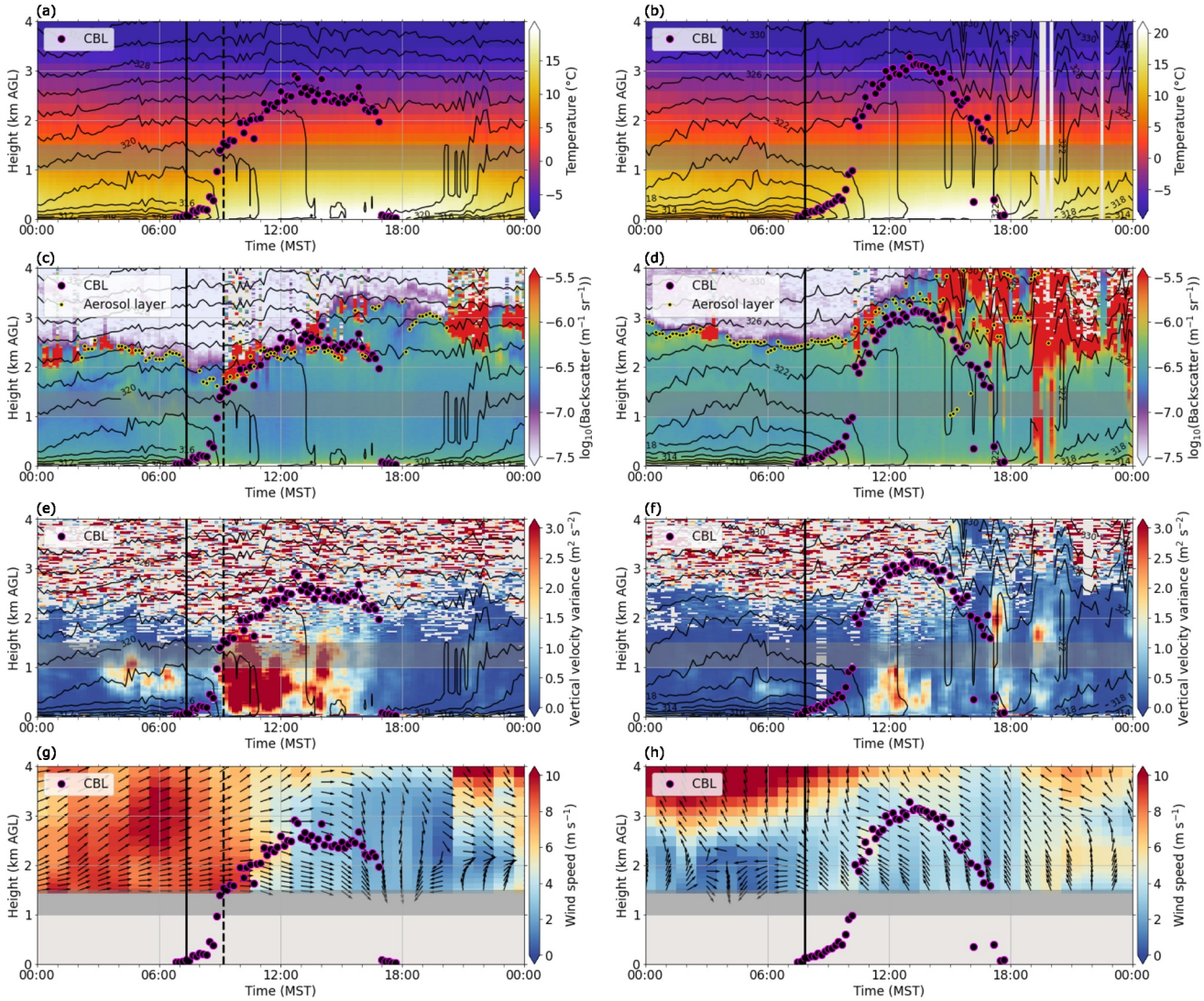

Figure 7. Time-height cross section of (a, b) air temperature retrieved with TROPoe, (c, d) backscatter from high spectral resolution lidar, (e, f) vertical velocity variance from Doppler lidar, (g, h) horizontal wind speed (color-coded) and wind vector (arrows) from RAP on a short upvalley (UV) wind day (7 August 2022, left column) and a long UV wind day (12 August 2022, right column). Black contours (a–f) represent potential temperature profiles retrieved with TROPoe. Magenta-black markers indicate convective boundary layer depth and yellow-black markers aerosol layer depth (c, d). The dark gray horizontal bar represents the characteristic ridge height. The vertical solid lines mark the objectively determined onset of UV wind at Gothic (mean between onset times at Avery Picnic and Kettle Ponds), and the vertical dashed line indicates the shift back to downvalley wind on the short UV wind day.

4.2. Diurnal Composites of Atmospheric Conditions During Short and Long Upvalley Wind Days

To investigate our hypothesis of forced channeling, which is based on the findings from the two case studies (Section 4.1), we computed 24-hr composites of several variables that we considered relevant. Consistent with Figure 5, mean wind direction turned to UV in the morning for both short and long UV wind days (Figure 8a). On short UV wind days, a sharp transition to DV flow occurred at around 10:00 MST on the average at both sites and hardly any UV flow was observed for the rest of the day. On long UV wind days, the UV flow persisted until midafternoon on average. Near-surface wind speed was quite weak during the night (<2 m s^{-1}) and gradually accelerated after the turn to UV wind (Figure 8b). No distinct differences are visible between days with short and long UV wind in the morning consistent with the findings from the case studies. Near-surface temperature and water vapor mixing ratio both increased after sunrise (Figures 8c and 8d). With the onset of UV wind, mixing ratio remained constant at Kettle Ponds and slightly decreased at Avery Picnic. This might be related to the growing CBL and the increase in turbulence during this time period (Figures 8e and 8g), mixing moist air from close to the

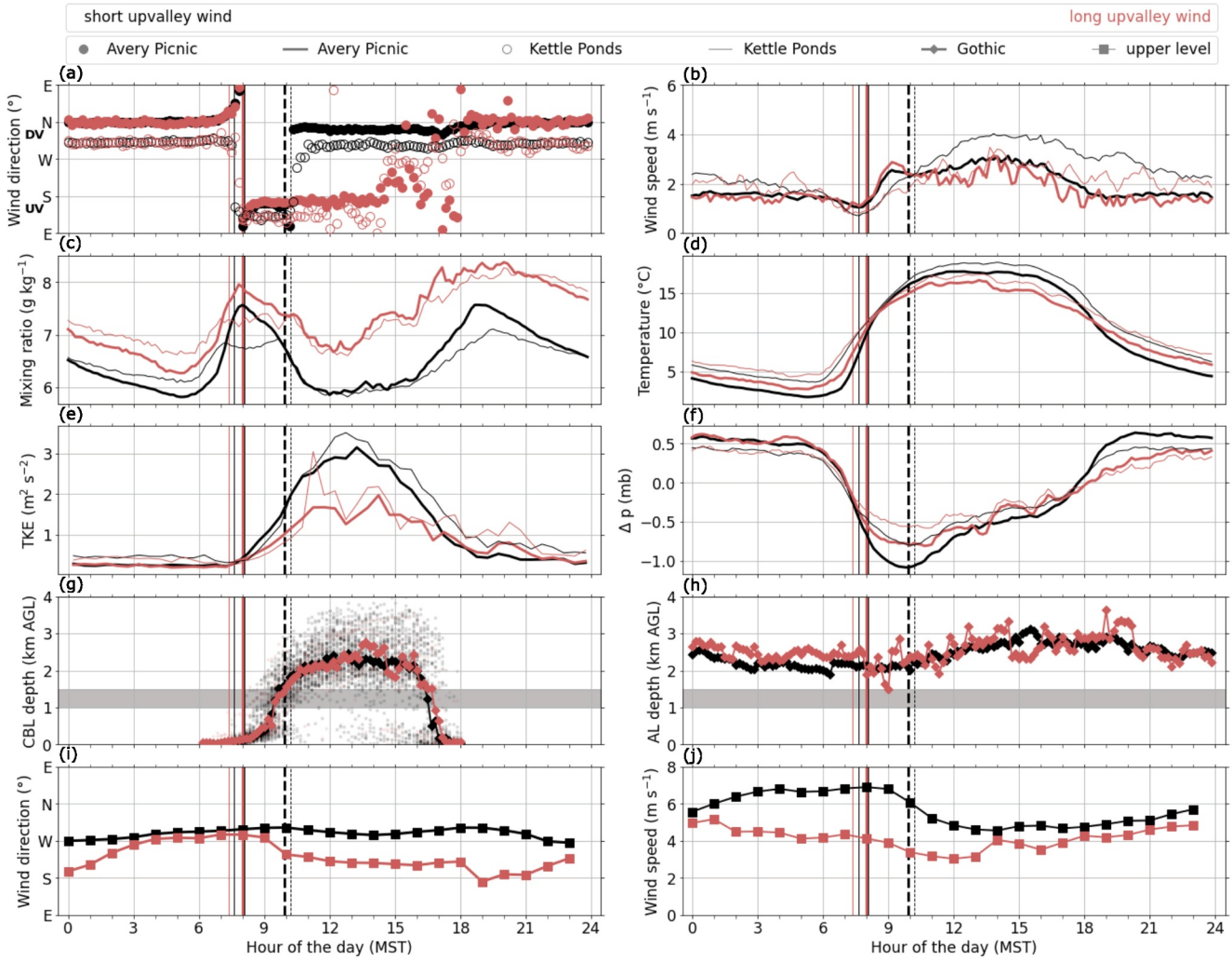

Figure 8. 24-hr mean composites of near-surface (a) wind direction (vector average), (b) wind speed, (c) water vapor mixing ratio, (d) temperature, and (e) turbulent kinetic energy (f) horizontal pressure gradient between Avery Picnic and Kettle Ponds in the upper part of the valley and Roaring Judy in the lower part of the valley after reducing the pressure at Roaring Judy to the altitude of the higher sites; (g) convective boundary layer (CBL) depth computed from TROPoe retrievals using the parcel method (median); (h) aerosol layer AL depth determined from the high spectral resolution lidar backscatter profiles (median); and upper-level (i) wind direction and (j) wind speed at 1.5 km above ground level from the RAP model for short (black) and long (red) upvalley (UV) wind days during the warm season. The dark gray horizontal bars in (g) and (h) represent the characteristic ridge height and small markers in (g) indicate individual CBL depths. The vertical solid thick and thin lines indicate the objectively determined onset of UV wind at Avery Picnic and Kettle Ponds and the vertical dashed thick and thin lines indicate the shift back to downvalley (DV) wind on the short UV wind days. Approximate DV and UV wind directions are indicated in (a).

surface over a deeper layer. Water vapor mixing ratio was generally higher on days with long UV wind perhaps indicative of different large-scale air mass regimes. Daytime CBL depth and aerosol layer depth were remarkably similar on average on short and long UV wind days with median CBL depth leveling out at around 2 km after noon and aerosol layer depth ranging between 2 and 3 km (Figures 8g and 8h). Very few days had CBL depths of less than 1.5 km (small markers in Figure 8g).

When the CBL depth reached around 1.5 km on average (Figure 8g), clear changes in near-surface conditions occurred for both types of days, which were similar to the patterns found for the case studies (Section 4.1). Near-surface water vapor mixing ratio sharply decreased by up to 1 g kg^{-1} on average at both sites over a period of around 1 hr (Figure 8c). Additionally, TKE increased further (Figure 8e). The rapid drying near the surface could be related to a sharp increase in CBL depth, which allowed mixing of moist air from close to the surface over a very deep layer and entrainment of drier air from above the ridge height. On short UV wind days, wind direction turned back to DV. The horizontal pressure gradient reached its minimum in the morning and slightly increased

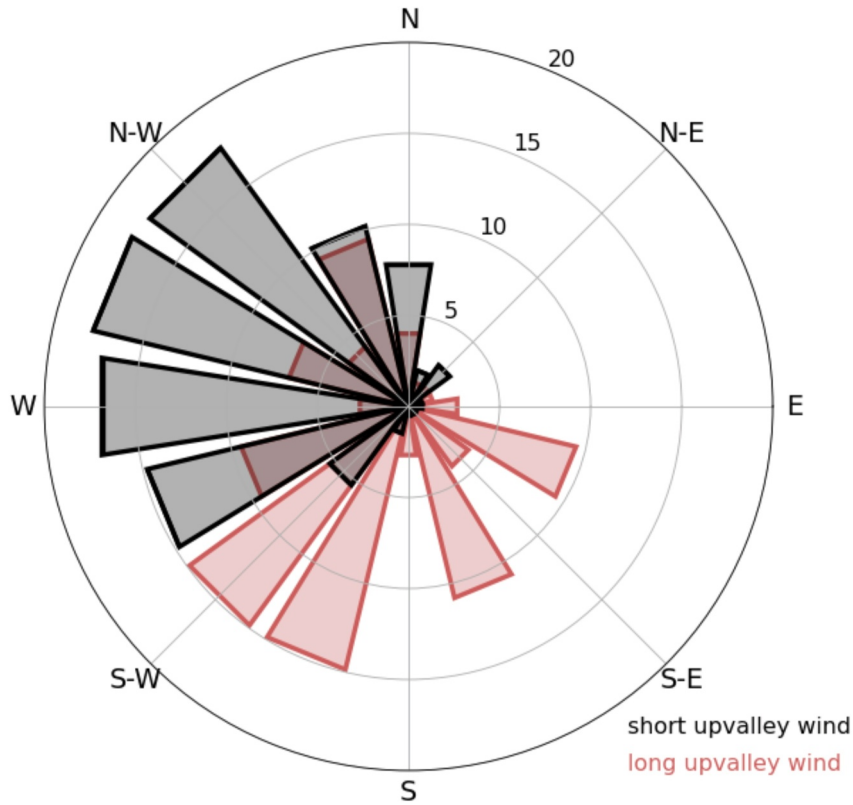

Figure 9. Wind rose of upper-level wind direction at ridge height (1.5 km above ground level) for short (black) and long (red) upvalley wind days during the warm season. Only data for the period 11:00 to 15:00 Mountain Standard Time are shown. The concentric circles indicates the percentage of how often a certain wind direction occurs for each type of days.

afterward (Figure 8f), deviating from the typical temporal evolution on thermally driven days found in other valleys (e.g., Giovannini et al., 2017; Lehner et al., 2019). The median CBL depth at the time of the onset of DV wind on short UV days was approximately 1.8 km; that is, it extended a few hundred meters above the mean ridge height.

Similar to the case studies, upper-level wind at 1.5 km AGL showed distinct differences between days with short and long UV wind (Figures 8i, 8j, and 9). Although the zonal component of the mean upper-level flow was positive (westerly) during both types of days, the flow had a northerly component on days with short UV wind and a southerly component on days with long UV wind on average. Differences in wind direction were especially evident during the day, when short UV wind days were almost exclusively associated with west-southwesterly to northerly upper-level flow and long UV wind days dominantly occurred when the flow was southwesterly to easterly (Figure 9). It is worth noting that Rudisill et al. (2025) found a dependence of clouds in the East River Valley on upper-level wind direction. During the warm season, clouds correlated with southwesterly flow at 500 mb that is indicative of monsoon flow bringing moist air into the area. This suggests that the cloud conditions in the valley are dependent on the same upper-level wind directions that are important for the valley winds with southwesterly flow favoring long UV wind days and clouds. Overall higher humidity on long UV wind days (Figure 8c) supports this hypothesis. Upper-level wind speeds were 1–2 m s^{-1} weaker on average on long UV wind days than on short UV wind days (Figure 8j). This could result in downward transport of weaker momentum and thus a weaker valley wind. However, we did not find clear observational evidence for this. While valley wind speed at Kettle Ponds was weaker on long UV wind days after midmorning, it was very similar at Avery Picnic on both types of days (Figure 8b).

The analysis of mean conditions confirms the findings of the case studies and strengthens our hypothesis of forced channeling being the responsible process for the early reversal of the UV wind on approximately 80% of all thermally driven days.

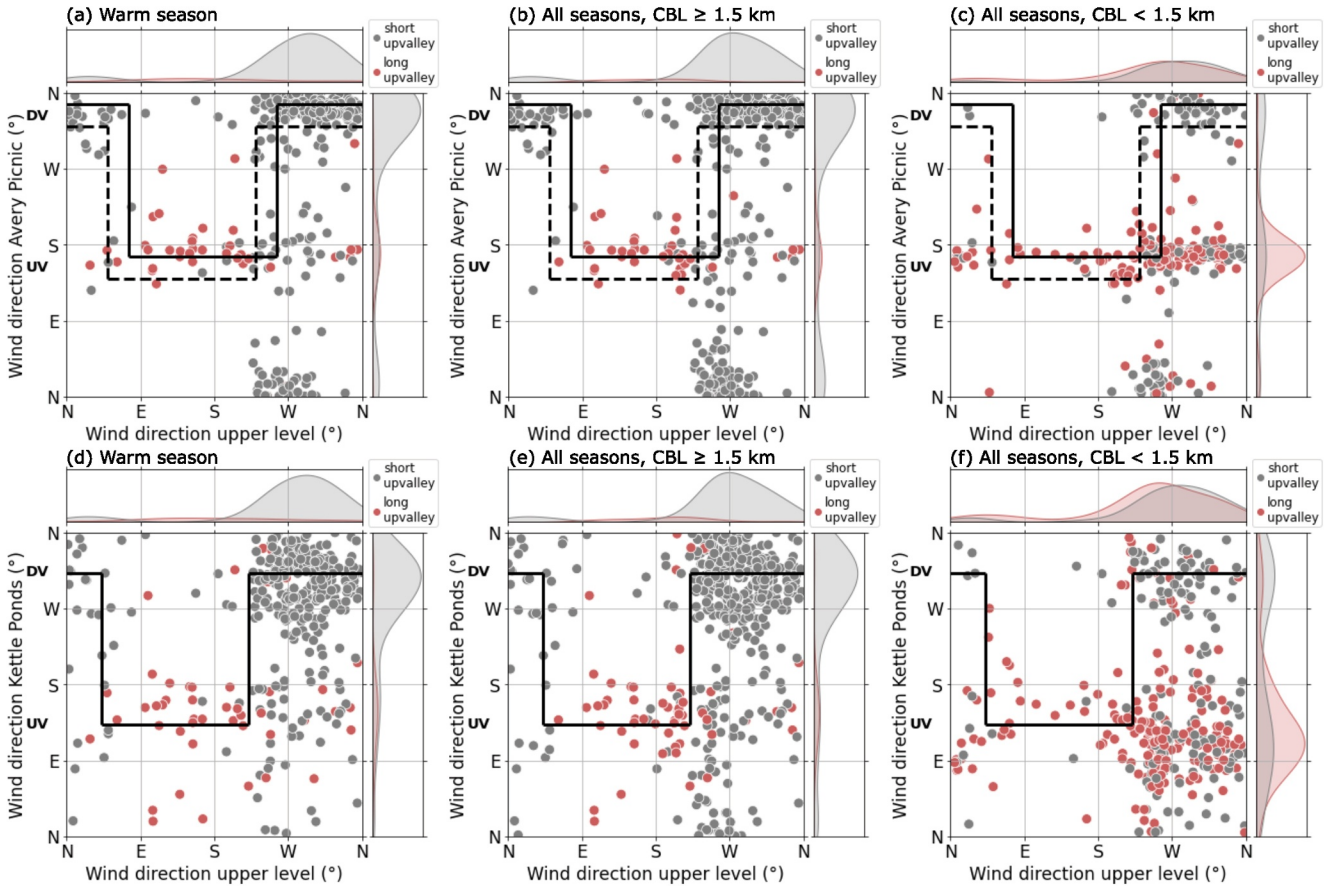

Figure 10. Relationship between the valley wind direction at Avery Picnic (a–c) and Kettle Ponds (d–f) and the upper-level wind at ridge height (1.5 km above ground level) during the period 11:00 to 15:00 Mountain Standard Time during short (gray) and long (red) upvalley wind days. (a, d) show days during the warm season, (b, e) show periods during all seasons when convective boundary layer (CBL) depth was larger than 1.5 km, and (c, f) show periods during all seasons when CBL depth was less than 1.5 km. The horizontal and vertical panels show the distribution of the upper-level and valley wind direction respectively. The solid black lines indicate the theoretical relationship for the forced channeling mechanisms based on the valley axis orientation near the surface. The dashed black lines in (a–c) additionally mark the theoretical relationship for the terrain-based northwest to southeast oriented valley axis at Avery Picnic.

5. Relationship Between Upper-Level Wind and Valley Wind Direction

To further investigate if the observed wind patterns in the upper East River Valley can be explained by the forced channeling mechanisms, we analyzed the relationship between upper-level wind direction at ridge height and valley wind direction near the surface on thermally driven days during the warm season. We considered the time period 11:00 to 15:00 MST when differences in valley wind direction for short and long UV wind days were most pronounced (Figure 8a). The most frequent upper-level wind direction was south-westerly to northerly (Figures 10a and 10d). Such upper-level flow direction was almost exclusively associated with northerly DV flow in the valley and occurred on days classified as short UV wind days (gray markers). On a few days, the upper-level wind direction had a southerly or southeasterly component. Under such upper-level flow direction, UV wind was present in the valley between 11:00 and 15:00 MST. These samples were classified as long UV wind days (red markers).

The black lines in Figure 10 indicate the theoretical lines for forced channeling following the concept of Whiteman and Doran (1993). The solid black lines are based on the valley axis direction determined from the observed near-surface UV wind direction at Avery Picnic and Kettle Ponds indicated by the solid gray lines in Figure 2c. The shift from a DV to UV regime did align fairly well with the theoretical lines based on the respective near-surface wind directions especially at Kettle Ponds. At Avery Picnic, there was a slight discrepancy. According to the theoretical line, southwesterly to westerly upper-level flow should result in forced channeling in southerly UV direction. However, the data clearly showed the predominance of northerly DV wind in the valley

for such upper-level flow direction. This might be related to the forking of the valley north of Avery Picnic and the overall orientation of the sidewalls (Figure 2c). Although the near-surface flow at Avery Picnic during the day had a south-southeasterly component for UV wind and a north-northwesterly component for DV wind (solid black line in Figure 10a), it is possible that the valley axis relevant for forced channeling is more northwesterly to southeasterly, which is more aligned with the overall orientation of the sidewalls. This theory is supported by the fact that the theoretical line (dashed black lines in Figures 10a–10c), which is based on the subjectively determined terrain-based valley axis (dashed gray line in Figure 2c), almost perfectly captures the shift from UV to DV wind when the upper-level flow direction crosses a southwesterly line.

The data suggest that the evolution of a deep CBL above ridge height is a necessary precondition for forced channeling in the upper East River Valley. But what happens when the CBL does not extend above ridge height? To investigate this, we extended our analysis of the 11:00 to 15:00 MST daytime period to all seasons. The CBL depth strongly depends on snow cover in the valley (Adler et al., 2023) and by including other seasons, maximum daytime CBL depths now also remained lower than the ridge height. Like for the warm season, we selected thermally driven days characterized by a clear shift from DV to UV wind around sunrise, excluding synoptically disturbed days or days when no UV wind formed due to high snow cover or clouds. We found 155 days with short UV wind and 71 days with long UV wind. Note that some days might be misclassified as short UV wind days because of the short daylight duration during peak winter (see local sunrise and sunset times in Figure 3).

Using 1.5 km as the critical CBL depth threshold, we compared valley and upper-level wind direction for periods with CBL depth above and below the threshold (Figures 10b, 10c, 10e, and 10f). When the CBL depth was larger than 1.5 km, UV flow was only able to persist under southerly upper-level flow (Figures 10b and 10e) consistent with what we observed for the warm season (Figures 10a and 10d). When the CBL depth was less than 1.5 km, the majority of cases now reveal UV wind at midday despite a southwesterly to northerly upper-level wind (Figures 10c and 10f). This can be explained by a decoupling of the valley atmosphere from the upper-level flow due to the low CBL depth, which allowed the persistence of thermally driven UV wind until the afternoon.

Our analysis was limited to days with a distinct thermally driven signal in the morning. On these days, the forced channeling mechanism dominated the valley flow evolution during the day when a deep CBL formed. If the criteria for day selection were relaxed, other mechanisms such as downward momentum transport or pressure driven channeling could also be present and alter the response of valley wind direction to upper-level wind direction (Figure 1). Mountain waves and wave breaking are also expected to occur under certain upper-level conditions and to impact mean and turbulent conditions in the valley (Eli Schwat, personal communication).

6. Discussion

The deep, relatively weak stably stratified residual layer with high aerosol loading seems to be an important precondition enabling the CBL at Gothic to grow far above ridge height. This aerosol layer was regularly present throughout the warm season and was only temporarily absent when synoptic systems moved through. It was usually capped by an elevated temperature inversion in which moisture decreased, best visible in the radiosonde profiles at 05:00 MST (Figure 11a). We expect that this aerosol layer did not form on the scale of the valley but was rather a feature present on the scale of the Rocky Mountains range. Plain-mountain circulations are known to efficiently transport aerosol and moisture upward from lower layers into the free troposphere over mountain ranges, leading to deep aerosol layers (e.g., Henne et al., 2004, 2005). These circulations have, for example, been detected over the European Alps (e.g., Lugauer & Winkler, 2005) and over the Rocky Mountains (e.g., Reiter & Tang, 1984). To investigate the horizontal extent of this deep weak stably stratified layer with high aerosol loading that was observed in the upper East River Valley, we compared temperature and water vapor mixing ratio profiles from radio soundings at Gothic to the profiles from the operational radio soundings at Grand Junction west of the main mountain range (Figure 2a). Although approximately 140 km away and around 1.5 km lower in elevation, temperature and water vapor mixing ratio profiles at Grand Junction were, on average, similar to the ones at Gothic above ridge height with a less stably stratified layer below around 5.5 km MSL (layer I in Figure 11) and a more stably stratified layer above (II). On the two days in August selected as case studies (Section 4.1), the aerosol layer extended up to around 5.5 km MSL at Gothic in the morning and was topped by a sharp temperature inversion in which water vapor mixing ratio rapidly decreased (Figure 11a). The radio

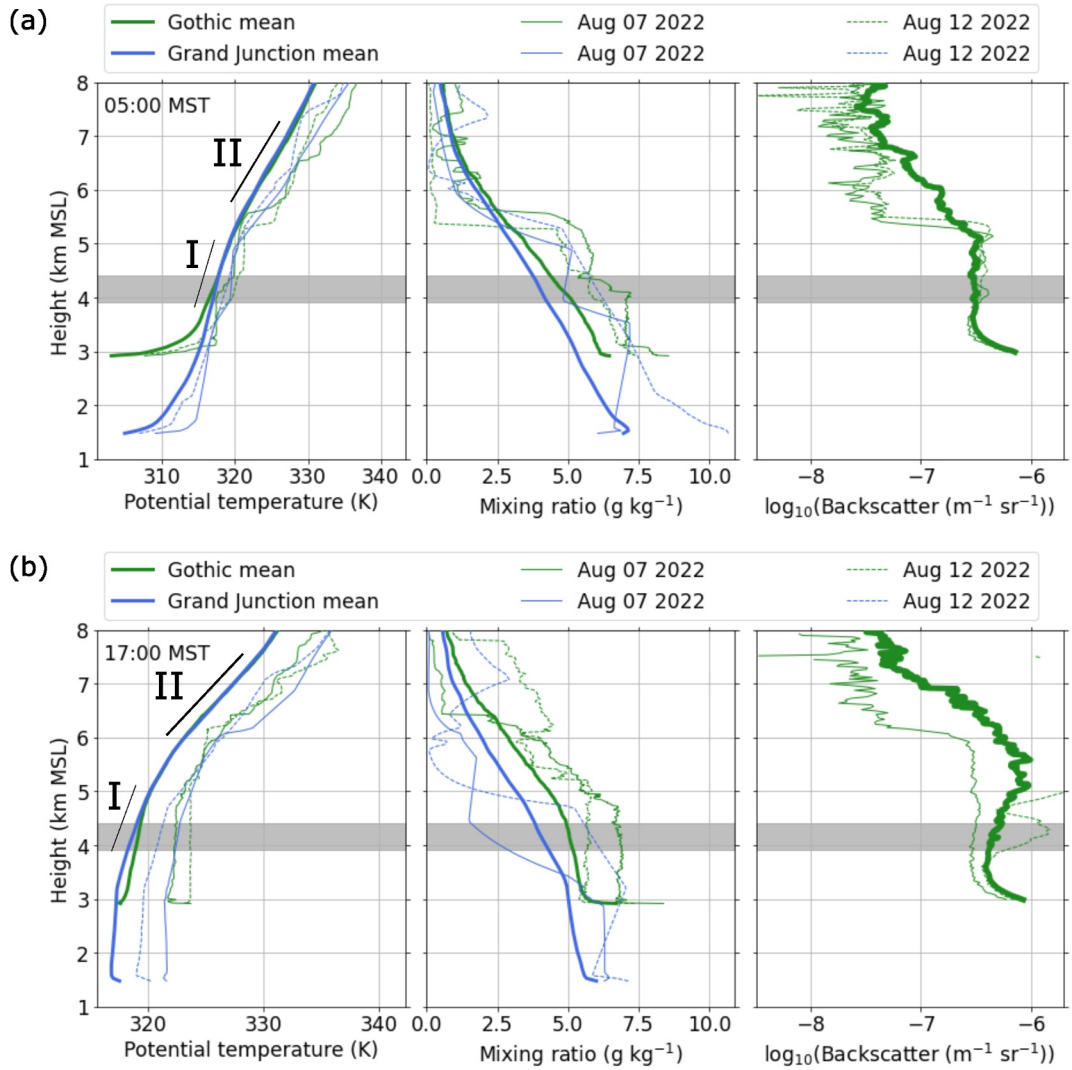

Figure 11. Profiles of potential temperature, water vapor mixing ratio, and backscatter on thermally driven days during the warm season in 2022 at Gothic in green and Grand Junction in blue (thick solid lines) and on two selected days (7 August 2022 (thin solid line) and August 12 (thin dashed line)). (a) shows the profiles at 05:00 Mountain Standard Time (MST) and (b) at 17:00 MST. Temperature and mixing ratio profiles are from radiosonde launches and backscatter profiles are from high spectral resolution lidar (Gothic only). The dark gray horizontal bar represents the characteristic ridge height and I and II denote a less and more stably stratified layer present at both sites.

soundings at Grand Junction indicated strong gradients in temperature and water vapor mixing ratio at the same height level indicating that a deep layer with higher moisture and likely higher aerosol content was present over a large area over and west of the Rocky Mountains. The top of the aerosol layer and associated gradients, especially in moisture, were less clear in the afternoon soundings and agree to a lesser extent between both sides (Figure 11b). This is likely due to the impact of local upward moisture transport, moist convection, and precipitation impacting the conditions at the intermountain site.

Although deep aerosol layers up to 4 km MSL extending far above the surrounding ridges have also been reported over the European Alps using airborne remote sensing observations (Henne et al., 2004), the CBL there usually does not grow to the top of the aerosol layer and often remains well below ridge height (e.g., Babić et al., 2024). Possible reasons for this difference compared to our findings for the East River Valley could be the lower available solar energy in the Alps due to their location at higher latitude, the partitioning of the available energy at the surface into sensible and latent heat flux due to the differences in land surface conditions and vegetation, valley orientation and exposure, altitude with respect to sea level, and other terrain characteristics. The overall

northwest-southeast orientation of the East River Valley favors sun exposure, which may contribute to the rapid growth of the CBL in the morning. Although the highest peaks of the Alps extend above 4 km MSL, similar to the Rocky Mountains, the valley floors in the Alps are typically at a much lower altitude often less than 1 km MSL, resulting in deeper valleys compared to the Rocky Mountains. The smaller valley depth combined with the higher altitude may make valleys in the Rocky Mountains more easily impacted by stronger midtropospheric winds, similar to high-altitude glacier valleys in the European Alps where thermally driven glacier flows are often eroded by the large-scale flow (Goger et al., 2022). A more detailed investigation of the processes impacting the CBL and aerosol layer evolution in both mountain regions is left for future studies.

The onset of UV wind in the upper part of the East River Valley in the morning is earlier than observed in other major valleys such as the Inn Valley and the Adige Valley, two heavily researched valleys in the European Alps. While UV wind onset in those valleys is around local noon (Giovannini et al., 2017; Lehner et al., 2019), UV wind onset in the East River Valley is detected within roughly two hours after sunrise when the along-valley pressure gradient starts to decreases in response to daytime warming. Possible explanations for the difference in timing could be the aforementioned differences in valley orientation and exposure as well as the surface energy balance, perhaps leading to a more rapid warming of the valley atmosphere after sunrise and a faster buildup of the along-valley pressure difference in the East River Valley. Other factors could be the valley dimension and the location of the measurement sites within the valley that were used in the observational studies. Observational studies in the Inn Valley usually focus on the area around the city of Innsbruck in the middle part of the more than 100 km long valley (e.g., Lehner et al., 2019; Vergeiner & Dreiseitl, 1987). Giovannini et al. (2017) investigated the valley wind in the more than 100 km long Adige Valley using several sites distributed along the valley floor and found that strength and timing of the UV wind varied along the valley axis with a slightly earlier reversal in the morning in the upper part of the valley. A numerical study for four major valleys in the Himalayas found a strong dependency of valley winds on location within the valley and local topography (Mikkola et al., 2023). This possible impact of site location on the timing of the UV wind onset is supported by wind measurements at Roaring Judy in the lower part of the East River Valley (Figure 2b), where the onset of UV wind is observed at around 09:00 MST on the average, that is, up to 2 hr later compared to Kettle Ponds and Avery Picnic in the upper part of the valley (not shown).

7. Summary and Conclusions

We analyzed the diurnal cycle of the flow and the boundary layer conditions in the high-altitude East River Valley in Colorado's Rocky Mountains for a nearly 2-year period using observations from the SAIL and SPLASH field campaigns. Especially during the warm season when the valley floor was not covered by snow, we observed an unexpected early reversal of thermally driven UV wind to DV wind in the upper part of the valley in mid to late morning on the majority of days. The aims of this study are to (a) characterize the boundary layer evolution and structure on days with an early reversal of UV to DV wind (short UV wind days) and without (long UV wind days) and (b) to identify the physical processes responsible for the early flow reversal.

On more than 75% of all days during the warm season, a typical thermally driven flow system was observed in the upper East River Valley in the early morning. The sketches in Figure 12 provide a graphical overview of the flow pattern evolution on such days. DV flow and a surface inversion were present before sunrise (Figure 12a). The flow turned to UV wind shortly after sunrise associated with the erosion of the nocturnal inversion by the development of a CBL (Figure 12b). This pattern was the same for short and long UV wind days. On approximately 80% of these thermally driven days the UV wind lasted only for a short period and the flow turned back to DV direction in midmorning (around 10:00 MST on average) (Figure 12c). This shift to DV wind occurred at the same time that the CBL grew above the height of the surrounding ridges reaching depths of 1.5–2 km above the valley floor. Simultaneously, near-surface water vapor mixing ratio sharply decreased and turbulence increased throughout the CBL, and the along-valley horizontal pressure gradient reached a local minimum and slightly increased afterward. Very similar CBL depths and changes in the boundary layer, except for the valley wind reversal, were observed on long UV wind days. The only distinct difference between both types of days laid in the upper-level wind direction at and above ridge height. On days with short UV wind, the upper-level wind direction was predominantly in the sector southwesterly to northerly (Figure 12c). On the few days with long UV wind, it had a stronger southerly component (Figure 12d).

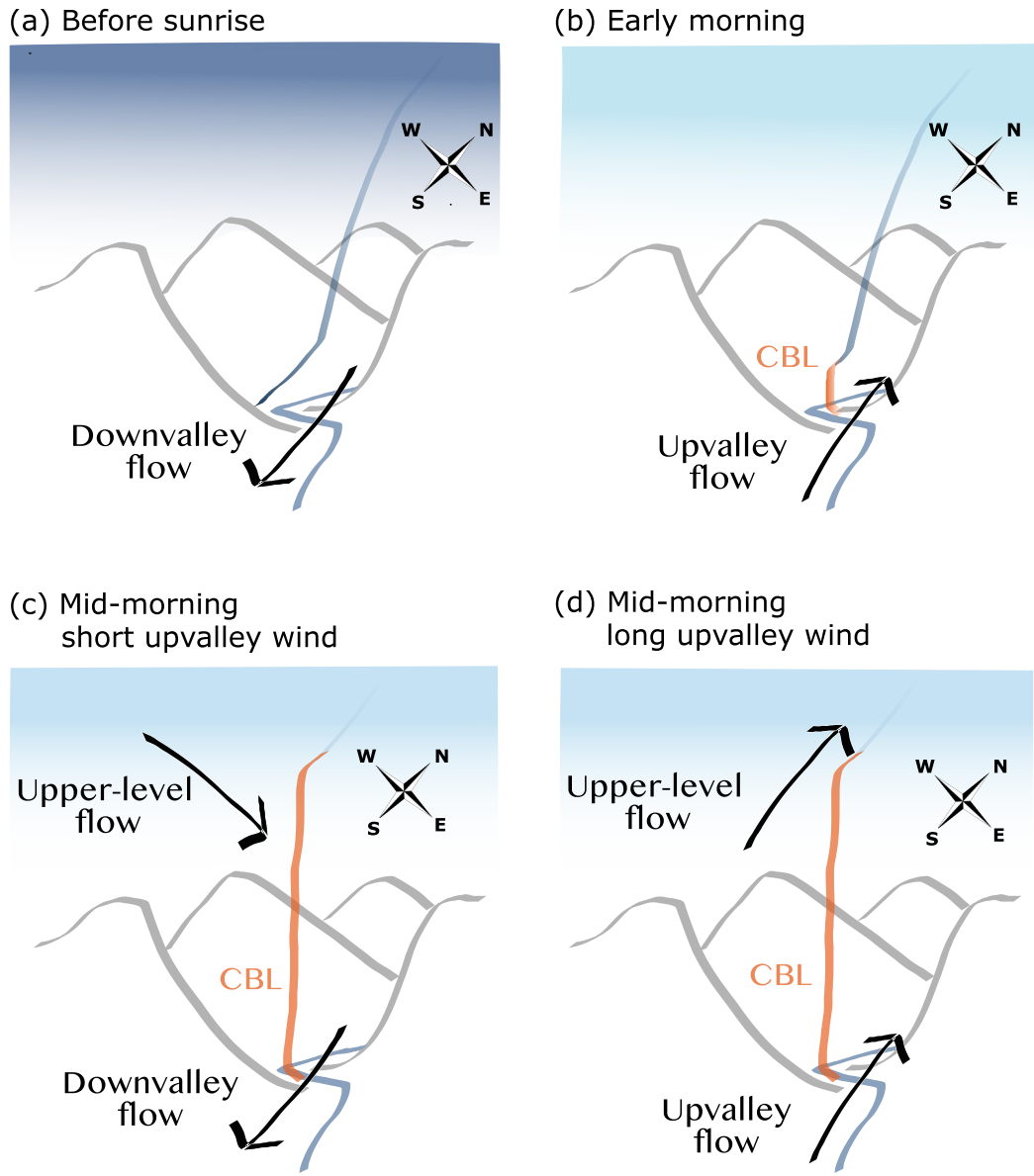

Figure 12. Graphical overview of the flow patterns in the upper East River Valley on days during the warm season when a thermally driven flow system is present in the morning. (a) Before sunrise, a nocturnal surface inversion and downvalley (DV) flow are present. (b) With the development of a convective boundary layer (CBL), the surface inversion is eroded and thermally driven upvalley (UV) wind starts. When the CBL grows above ridge height in midmorning, upper-level momentum is downward transported in the valley and channeled in (c) DV direction when the upper-level flow is southwesterly to northerly (short UV wind day) or in (d) UV direction when the upper-level flow has a southerly component (long UV wind day).

The observed relationship between the valley wind direction and the upper-level wind direction suggests that the forced channeling mechanism (Whiteman & Doran, 1993) determines the daytime flow pattern in the upper East River Valley on the selected days as soon as the CBL grows above ridge height. Hence, the flow pattern is a combination of thermally driven flow in the early morning and forced channeling afterward. On days when the upper-level flow direction is southwesterly to northerly, channeling occurs in DV direction (Figure 12c) ending the brief period with thermally driven UV flow that forms as long as the CBL is shallow and does not extend above ridge height (Figure 12b). On days when the upper-level flow has a stronger southerly component, the flow is channeled in UV direction and is not distinguishable from a thermally driven UV flow (Figure 12d). Since

southwesterly to northerly upper-level flow occurs much more frequently than southerly flow, short UV wind days dominate.

The forced channeling mechanism requires a deep well-mixed layer to couple the upper-level flow with the valley atmosphere. Such a layer was regularly present during the warm season when the CBL grew to the top of a deep weakly stably stratified residual layer with high aerosol content that extended up to 3 km above the valley floor (more than 5 km MSL) and likely was part of a mountain-scale circulation. Outside the warm season when the valley floor was partially or completely covered by snow, the CBL often remained lower and did not grow above ridge height. Under such conditions, UV flow persisted in the valley despite a southwesterly to northerly upper-level flow. This means that the valley atmosphere was decoupled from the upper levels preventing the forced channeling mechanism from occurring.

The distinct valley flow pattern on short and long UV wind days may impact how water vapor and aerosols are transported along the valley axis and to what extent they are vented above the ridges. They may also influence timing and location of moist convection initiation by inducing horizontal convergence over slopes and ridges. Strong turbulence in the boundary layer and entrainment of warm air from aloft may impact sublimation and melting of snow in spring with implications for streamflow runoff.

Our results highlight the importance of upper-air observations for studies in mountainous terrain. Only by analyzing near-surface conditions along with the thermodynamic and dynamic vertical structure in the boundary layer and above were we able to identify the processes responsible for the unexpected behavior of the near-surface flow in the valley. One of the challenges we faced in this high-altitude environment was the low backscatter content limiting the range of active remote sensing instruments, such as the Doppler lidar for wind retrievals or ceilometer for the detection of aerosol layers. Only the higher sensitivity of the HSRL allowed us to link the residual layer and CBL depth with the aerosol layer depth. The thermodynamic profiles retrieved from the passive infrared spectrometer proved to be invaluable for capturing the boundary layer stratification including the nocturnal surface inversion and the growth of the CBL during daytime.

Data Availability Statement

Measurements at Gothic are part of the Atmospheric Radiation Measurement (ARM) Mobile Facility (AMF2). The used data at Gothic are thermodynamic profiles retrieved with TROPoe from infrared spectrometer radiances (Turner, 2021), high spectral resolution lidar particulate backscatter profiles (Holz et al., 2021), Doppler lidar vertical velocity variance profiles (Shippert et al., 2021), and radiosonde profiles (Burk, 2021). Radiosonde profiles at Grand Junction were downloaded from the website University of Wyoming (University of Wyoming—Department of Atmospheric Science, 2024). NOAA Global Monitoring Laboratory conducted the ceilometer (Telg et al., 2024) and radiation (Soldo et al., 2023) measurements at Kettle Ponds. NOAA Air Resources Laboratory operated the 10-m flux tower at Kettle Ponds. NOAA Physical Sciences Laboratory conducted the Atmospheric Surface Flux Stations (ASFS) measurements at Avery Picnic (Cox et al., 2023) and surface meteorology measurements at Roaring Judy (Ballard et al., 2023). RAP model data are available from the National Oceanic and Atmospheric Administration (NOAA), Department of Commerce.

Acknowledgments
Funding for this work was provided by the NOAA Physical Sciences Laboratory, the U.S. Department of Energy (DOE) Office of Energy Efficiency and Renewable Energy, Wind Energy Technologies Office, and by the NOAA Atmospheric Science for Renewable Energy (ASRE) program. This research was supported by NOAA cooperative agreement NA22OAR4320151 for the Cooperative Institute for Earth System Research and Data Science (CIESRDS) and DOE's Atmospheric Systems Research Awards DE-SC0024266 and DE-SC0024082. This material is based upon work supported by the NSF National Center for Atmospheric Research, which is a major facility sponsored by the U.S. National Science Foundation under Cooperative Agreement No. 1852977. We thank all of the individuals, in particular Rocky Mountain Biological Laboratory (RMBL), for help with the SPLASH site selection, leases, instrument deployment and maintenance, data collection, and data quality control. The statements, findings, conclusions, and recommendations are those of the authors and do not necessarily reflect the views of NOAA or the U.S. Department of Commerce.

References

Adler, B., Turner, D. D., Bianco, L., Djalalova, I. V., Myers, T., & Wilczak, J. M. (2024). Improving solution availability and temporal consistency of an optimal-estimation physical retrieval for ground-based thermodynamic boundary layer profiling. *Atmospheric Measurement Techniques*, *17*(22), 6603–6624. https://doi.org/10.5194/amt-17-6603-2024

Adler, B., Wilczak, J. M., Bianco, L., Bariteau, L., Cox, C. J., de Boer, G., et al. (2023). Impact of seasonal snow-cover change on the observed and simulated state of the atmospheric boundary layer in a high-altitude mountain valley. *Journal of Geophysical Research: Atmospheres*, *128*(12), e2023JD038497. https://doi.org/10.1029/2023JD038497

Babić, N., Adler, B., Gohm, A., Lehner, M., & Kalthoff, N. (2024). Exploring the daytime boundary layer evolution based on Doppler spectrum width from multiple coplanar wind lidars during CROSSINN. *Weather and Climate Dynamics*, *5*(2), 609–631. https://doi.org/10.5194/wcd-5-609-2024

Ballard, B., Gottas, D., & White, A. (2023). NOAA PSL surface meteorology Roaring Judy for SPLASH [Dataset]. *Zenodo*. https://doi.org/10.5281/zenodo.10392121

Benjamin, S. G., Weygandt, S. S., Brown, J. M., Hu, M., Alexander, C. R., Smirnova, T. G., et al. (2016). A North American hourly assimilation and model forecast cycle: The Rapid Refresh. *Monthly Weather Review*, *144*(4), 1669–1694. https://doi.org/10.1175/MWR-D-15-0242.1

Bianco, L., Adler, B., Bariteau, L., Djalalova, I. V., Myers, T., Pezoa, S., et al. (2024). Sensitivity of thermodynamic profiles retrieved from ground-based microwave and infrared observations to additional input data from active remote sensing instruments and numerical weather prediction models. *Atmospheric Measurement Techniques*, *2024*, 1–26. https://doi.org/10.5194/amt-2023-263

Blumberg, W., Turner, D., Löhnert, U., & Castleberry, S. (2015). Ground-based temperature and humidity profiling using spectral infrared and microwave observations. Part II: Actual retrieval performance in clear-sky and cloudy conditions. *Journal of Applied Meteorology and Climatology*, *54*(11), 2305–2319. https://doi.org/10.1175/JAMC-D-15-0005.1

Burk, K. (2021). Balloon-borne sounding system (SONDEWNPN). 2021-09-01 to 2023-06-16 [Dataset]. *ARM Mobile Facility (GUC) Gunnison, CO; AMF2 (main site for SAIL) (M1)*. https://doi.org/10.5439/1595321

Caicedo, V., Delgado, R., Sakai, R., Knepp, T., Williams, D., Cavender, K., et al. (2020). An automated common algorithm for planetary boundary layer retrievals using aerosol lidars in support of the US EPA photochemical assessment monitoring stations program. *Journal of Atmospheric and Oceanic Technology*, *37*(10), 1847–1864. https://doi.org/10.1175/JTECH-D-20-0050.1

Carrera, M. L., Gyakum, J. R., & Lin, C. A. (2009). Observational study of wind channeling within the St. Lawrence River Valley. *Journal of Applied Meteorology and Climatology*, *48*(11), 2341–2361. https://doi.org/10.1175/2009JAMC2061.1

Cox, C. J., Gallagher, M., Intrieri, J., Butterworth, B., Meyers, T., & Persson, O. (2023). Atmospheric surface flux station #50 measurements (level 2 processed), study of precipitation, the lower atmosphere and surface for hydrometeorology (SPLASH), October 2021–June 2023 [Dataset]. *Zenodo*. https://doi.org/10.5281/zenodo.10313364

Cox, C. J., Intrieri, J. M., Butterworth, B. J., de Boer, G., Gallagher, M. R., Hamilton, J., et al. (2025). Observations of surface energy fluxes and meteorology in the seasonally snow-covered high-elevation East River watershed during SPLASH, 2021–2023. *Earth System Science Data*, *17*, 1481–1499. https://doi.org/10.5194/essd-17-1481-2025

de Boer, G., White, A., Cifelli, R., Intrieri, J., Abel, M. R., Mahoney, K., et al. (2023). Supporting advancement in weather and water prediction in the upper Colorado River basin: The SPLASH campaign. *Bulletin America Meteorology Social*, *104*(10), E1853–E1874. https://doi.org/10.1175/BAMS-D-22-0147.1

Duncan, J. B., Jr., Bianco, L., Adler, B., Bell, T., Djalalova, I. V., Riihimaki, L., et al. (2022). Evaluating convective planetary boundary layer height estimations resolved by both active and passive remote sensing instruments during the CHEESEHEAD19 field campaign. *Atmospheric Measurement Techniques*, *15*(8), 2479–2502. https://doi.org/10.5194/amt-15-2479-2022

Eckman, R. M. (1998). Observations and numerical simulations of winds within a broad forested valley. *Journal of Applied Meteorology and Climatology*, *37*(2), 206–219. https://doi.org/10.1175/1520-0450(1998)037⟨0206:OANSOW⟩2.0.CO;2

Eloranta, E. E. (2005). High spectral resolution lidar. In *Lidar: Range-resolved optical remote sensing of the atmosphere* (pp. 143–163). Springer. https://doi.org/10.1007/0-387-25101-4_5

Feldman, D. R., Aiken, A. C., Boos, W. R., Carroll, R. W. H., Chandrasekar, V., Collis, S., et al. (2023). The Surface Atmosphere Integrated Field Laboratory (SAIL) campaign. *Bulletin of the American Meteorological Society*, *104*, E2192–E2222. https://doi.org/10.1175/BAMS-D-22-0049.1

Giovannini, L., Laiti, L., Serafin, S., & Zardi, D. (2017). The thermally driven diurnal wind system of the Adige Valley in the Italian Alps. *Quarterly Journal of the Royal Meteorological Society*, *143*(707), 2389–2402. https://doi.org/10.1002/qj.3092

Goger, B., Stiperski, I., Nicholson, L., & Sauter, T. (2022). Large-eddy simulations of the atmospheric boundary layer over an Alpine glacier: Impact of synoptic flow direction and governing processes. *Quarterly Journal of the Royal Meteorological Society*, *148*(744), 1319–1343. https://doi.org/10.1002/qj.4263

Goldsmith, J. (2016). *High spectral resolution lidar (HSRL) instrument handbook* (Tech. Rep.). DOE Office of Science Atmospheric Radiation Measurement (ARM) Program (United States). https://doi.org/10.2172/1251392

Hall, D. K., & Riggs, G. A. (2021). *MODIS/Terra snow cover daily L3 global 500m SIN grid, version 61*, NASA National Snow and Ice Data Center Distributed Active Archive Center. https://doi.org/10.5067/MODIS/MOD10A1.061

Henne, S., Furger, M., Nyeki, S., Steinbacher, M., Neininger, B., De Wekker, S., et al. (2004). Quantification of topographic venting of boundary layer air to the free troposphere. *Atmospheric Chemistry and Physics*, *4*(2), 497–509. https://doi.org/10.5194/acp-4-497-2004

Henne, S., Furger, M., & Prévôt, A. S. (2005). Climatology of mountain venting–induced elevated moisture layers in the lee of the Alps. *Journal of Applied Meteorology*, *44*(5), 620–633. https://doi.org/10.1029/2005JD005936

Holdridge, D. (2020). *Balloon-borne sounding system (SONDE) instrument handbook* (Tech. Rep.). DOE Office of Science Atmospheric Radiation Measurement (ARM) Program (United States). https://doi.org/10.2172/1020712

Holz, R., Garcia, J., Schuman, E., Bambha, R., Ermold, B., Eloranta, E., & Garcia, J. (2021). High spectral resolution lidar (HSRL). 2021-09-01 to 2023-06-15 [Dataset]. *ARM Mobile Facility (GUC) Gunnison, CO; AMF2 (main site for SAIL) (M1)*. https://doi.org/10.5439/1462207

Jackson, P. L., Mayr, G., & Vosper, S. (2013). Dynamically-driven winds. In F. K. Chow, S. F. De Wekker, & B. J. Snyder (Eds.), *Mountain weather research and forecasting* (pp. 121–218). Springer. https://doi.org/10.1007/978-94-007-4098-3_3

Kirshbaum, D. J., Adler, B., Kalthoff, N., Barthlott, C., & Serafin, S. (2018). Moist orographic convection: Physical mechanisms and links to surface-exchange processes. *Atmosphere*, *9*(3), 80. https://doi.org/10.3390/atmos9030080

Knuteson, R. O., Revercomb, H. E., Best, F. A., Ciganovich, N. C., Dedecker, R. G., Dirkx, T. P., et al. (2004a). Atmospheric emitted radiance interferometer. Part II: Instrument performance. *Journal of Atmospheric and Oceanic Technology*, *21*(12), 1777–1789. https://doi.org/10.1175/JTECH-1663.1

Knuteson, R. O., Revercomb, H. E., Best, F. A., Ciganovich, N. C., Dedecker, R. G., Dirkx, T. P., et al. (2004b). Atmospheric emitted radiance interferometer. Part I: Instrument design. *Journal of Atmospheric and Oceanic Technology*, *21*(12), 1763–1776. https://doi.org/10.1175/JTECH-1662.1

Lehner, M., Rotach, M. W., & Obleitner, F. (2019). A method to identify synoptically undisturbed, clear-sky conditions for valley-wind analysis. *Boundary-Layer Meteorology*, *173*(3), 435–450. https://doi.org/10.1007/s10546-019-00471-2

Lehner, M., Rotach, M. W., Sfyri, E., & Obleitner, F. (2021). Spatial and temporal variations in near-surface energy fluxes in an alpine valley under synoptically undisturbed and clear-sky conditions. *Quarterly Journal of the Royal Meteorological Society*, *147*(737), 2173–2196. https://doi.org/10.1002/qj.4016

Lugauer, M., & Winkler, P. (2005). Thermal circulation in South Bavaria-climatology and synoptic aspects. *Meteorologische Zeitschrift*, *14*(1), 15–30. https://doi.org/10.1127/0941-2948/2005/0014-0015

Lundquist, J. D., Vano, J., Gutmann, E., Hogan, D., Schwat, E., Haugeneder, M., et al. (2024). Sublimation of snow. *Bulletin America Meteorology Social*, *105*(6), E975–E990. https://doi.org/10.1175/BAMS-D-23-0191.1

Mikkola, J., Sinclair, V. A., Bister, M., & Bianchi, F. (2023). Daytime along-valley winds in the Himalayas as simulated by the weather research and forecasting (WRF) model. *Atmospheric Chemistry and Physics*, *23*(2), 821–842. https://doi.org/10.5194/acp-23-821-2023

Newsom, R. K., & Krishnamurthy, R. (2022). *Doppler lidar (DL) instrument handbook* (Tech. Rep.). DOE Office of Science Atmospheric Radiation Measurement (ARM) Program (United States). https://doi.org/10.2172/1034640

Pal, S., Lee, T., Phelps, S., & De Wekker, S. (2014). Impact of atmospheric boundary layer depth variability and wind reversal on the diurnal variability of aerosol concentration at a valley site. *Science of the Total Environment*, *496*, 424–434. https://doi.org/10.1016/j.scitotenv.2014.07.067

Reiter, E. R., & Tang, M. (1984). Plateau effects on diurnal circulation patterns. *Monthly Weather Review*, *112*(4), 638–651. https://doi.org/10.1175/1520-0493(1984)112⟨0638:PEODCP⟩2.0.CO;2

Rudisill, W., Feldman, D., Cox, C. J., Riihimaki, L., & Sedlar, J. (2025). Seasonality and albedo dependence of cloud radiative forcing in the Upper Colorado River Basin. *Journal of Geophysical Research: Atmospheres*, *130*(6), e2024JD042366. https://doi.org/10.1029/2024JD042366

Sedlar, J., Riihimaki, L. D., Turner, D. D., Duncan, J., Adler, B., Bianco, L., et al. (2022). Investigating the impacts of daytime boundary layer clouds on surface energy fluxes and boundary layer structure during CHEESEHEAD19. *Journal of Geophysical Research: Atmospheres*, *127*(5), e2021JD036060. https://doi.org/10.1029/2021JD036060

Seibert, P., Beyrich, F., Gryning, S.-E., Joffre, S., Rasmussen, A., & Tercier, P. (2000). Review and intercomparison of operational methods for the determination of the mixing height. *Atmospheric Environment*, *34*(7), 1001–1027. https://doi.org/10.1016/S1352-2310(99)00349-0

Shippert, T., Newsom, R., Riihimaki, L., & Zhang, D. (2021). Doppler lidar wind statistics profiles (DLPROFWSTATS4NEWS). 2021-09-01 to 2023-06-14 [Dataset]. *ARM Mobile Facility (GUC) Gunnison, CO; AMF2 (main site for SAIL) (M1)*. https://doi.org/10.5439/1178583

Soldo, L., Stierle, S., Hageman, D., Hall, E., Herrera, C., Hodges, G., et al. (2023). NOAA GML Kettle Ponds surface radiation budget and near-surface meteorology data for SPLASH [Dataset]. *Zenodo*. https://doi.org/10.5281/zenodo.10011476

Steyn, D. G., De Wekker, S. F. J., Kossmann, M., & Martilli, A. (2013). Boundary layers and air quality in mountainous terrain. In F. K. Chow, S. F. J. De Wekker, & B. J. Snyder (Eds.), *Mountain weather research and forecasting: Recent progress and current challenges* (pp. 261–289). https://doi.org/10.1007/978-94-007-4098-3_5

Telg, H., Sedlar, J., Herrera, C., & Stierle, S. (2024). NOAA GML and CIRES/uni. Of Colorado-Boulder ceilometer cloud data products at Kettle Ponds (CKP) for SPLASH [Dataset]. *Zenodo*. https://doi.org/10.5281/zenodo.10520198

Turner, D. D. (2021). Tropospheric optimal estimation retrieval (TROPoe). 2021-09-01 to 2023-06-10 [Dataset]. *ARM Mobile Facility (GUC) Gunnison, CO; AMF2 (main site for SAIL) (M1)*. https://doi.org/10.5439/1996977

Turner, D. D., & Blumberg, W. G. (2019). Improvements to the AERIoe thermodynamic profile retrieval algorithm. *IEEE Journal of Selected Topics in Applied Earth Observations and Remote Sensing*, *12*(5), 1339–1354. https://doi.org/10.1109/JSTARS.2018.2874968

Turner, D. D., & Löhnert, U. (2014). Information content and uncertainties in thermodynamic profiles and liquid cloud properties retrieved from the ground-based atmospheric emitted radiance interferometer (AERI). *Journal of Applied Meteorology and Climatology*, *53*(3), 752–771. https://doi.org/10.1175/JAMC-D-13-0126.1

Turner, D. D., & Löhnert, U. (2021). Ground-based temperature and humidity profiling: Combining active and passive remote sensors. *Atmospheric Measurement Techniques*, *14*(4), 3033–3048. https://doi.org/10.5194/amt-14-3033-2021

University of Wyoming—Department of Atmospheric Science. (2024). Upper air sounding information. Retrieved from https://weather.uwyo.edu/upperair/sounding.html

Vergeiner, I., & Dreiseitl, E. (1987). Valley winds and slope winds—Observations and elementary thoughts. *Meteorology and Atmospheric Physics*, *36*(1–4), 264–286. https://doi.org/10.1007/BF01045154

Weber, R. O., & Kaufmann, P. (1998). Relationship of synoptic winds and complex terrain flows during the MISTRAL field experiment. *Journal of Applied Meteorology and Climatology*, *37*(11), 1486–1496. https://doi.org/10.1175/1520-0450(1998)037⟨1486:ROSWAC⟩2.0.CO;2

Whiteman, C. D., & Doran, J. C. (1993). The relationship between overlying synoptic-scale flows and winds within a valley. *Journal of Applied Meteorology*, *32*(11), 1669–1682. https://doi.org/10.1175/1520-0450(1993)032⟨1669:TRBOSS⟩2.0.CO;2

Zardi, D., & Whiteman, C. D. (2013). Diurnal mountain wind systems. In F. K. Chow, S. F. J. De Wekker, & B. J. Snyder (Eds.), *Mountain weather research and forecasting* (pp. 35–119). Springer. https://doi.org/10.1007/978-94-007-4098-3_2